J. Earth Syst. Sci. (2020) 129:178
https://doi.org/10.1007/s12040-020-01430-z

An efficient global optimization method for self-potential data inversion using micro-differential evolution

SUNGKONO

Departement of Physics, Institut Teknologi Sepuluh Nopember, Kampus ITS Sukolilo, Surabaya 60111, Indonesia.
e-mail: hening_1@physics.its.ac.id

MS received 11 January 2020; revised 28 April 2020; accepted 29 April 2020; published online 28 August 2020

Self-potential (SP) method has many applications, where the interpretation of SP data can be used for qualitative and quantitative interpretation. However, inversion of SP data in this paper is of quantitative interpretation and consists of highly non-linear, multimodal data and deploys global optimum method (GOM). Micro-differential evolution (MDE) is a GOM with small or micro-population size (5–8 populations) for each iteration. Consequently, this approach involves small numbers of forward computation in the inversion process. Two MDE variants, including adaptive MDE (μJADE) and vectorized random mutation factor (MVDE) were tested first for different level of noises containing synthetic SP data with single anomaly and applied to synthetic SP data of multiple anomalies. The MDE variants are reliable and effective for inverting noisy SP data. Furthermore, in order to check the rationality of MDE variants, the algorithm is applied to seven field data from different applications, including groundwater exploration, shear zone tracing, water accumulation in landslides and embankment stability assessment. The model parameters revealed by MDE variants are accurate and show good agreement with the previous results estimated using other approaches. In addition, MDE variants also require fewer forward modelling calculations than other optimization approaches.

Keywords. Multiple anomalies; model parameters; uncertainty analysis; fast inversion; micro-population.

1. Introduction

Self-potential (SP) method is a passive geophysical method which measures natural potentials. The potential is usually produced by electrokinetic, electrochemical, and thermoelectric sources. Hence, the SP method has wide applications including cavity identification (Jardani *et al.* 2006), landslide study (Lapenna *et al.* 2003; Sungkono and Warnana 2018), embankment leakage detection (Moore *et al.* 2011; Sungkono and Warnana 2018), mineral and geothermal exploration (Biswas and Sharma 2014a; Byrdina *et al.* 2012), landfill leachate identification (Arora *et al.* 2007), and groundwater investigations (Monteiro Santos *et al.* 2002). SP method is often successful in producing both qualitative and quantitative interpretations in single and multiple anomalies.

Interpretation of SP data can be classified into two sections, signal analysis and an inversion process. In the first section, SP data is considered as a signal, which is then analyzed using signal analysis method, for example, continuous wavelet transform (Saracco *et al.* 2004), Euler deconvolution

(Agarwal and Srivastava 2009) and Hilbert transform (Sundararajan and Srinivas 1996), etc. Meanwhile in the second section, SP anomaly is analyzed using inversion approach. Two methods have been applied in inverting SP data such as local optimization (Srigutomo *et al.* 2006; Candra *et al.* 2014; Mehanee 2014) and GOM. Several GOMs have been successfully applied to SP anomaly inversion including differential evolution (DE) (Li and Yin 2012; Balkaya 2013), particle swarm optimization (PSO) (Monteiro Santos 2010; Pekşen *et al.* 2011), joint genetic-price algorithm (GPA) (Di Maio *et al.* 2016), very fast simulated annealing (VFSA) (Biswas and Sharma 2014b), genetic algorithm (GA) (Göktürkler and Balkaya 2012), black hole algorithm (BHA) (Sungkono and Warnana 2018), whale optimization algorithm (WOA) (Abdelazeem *et al.* 2019), and neural network (NN) (El-Kaliouby and Al-Garni 2009). However, three algorithms, namely NN, GA, and DE have not been studied yet for interpreting multi-anomaly of SP data.

DE is more effective and robust than PSO and GA for self-potential anomaly inversion (Balkaya 2013). However, DE also succeed for determining model parameters for gravity and magnetic anomalies (Ekinci *et al.* 2016, 2017, 2019, 2020; Balkaya *et al.* 2017). Nevertheless, DE algorithm generally uses a large population size for finding reasonable results, while giving a higher exploration capability to the optimizer for finding global solutions (Salehinejad *et al.* 2016, 2017). Therefore, using algorithms with a large population size for inversion process may not be suitable for highly time-consuming forward modelling calculations and for large number size of model parameters. Consequently, a DE algorithm with smaller population size for inversion process is required. Recently, micro-DE (MDE) variants have been proposed (Ren *et al.* 2010; Olguín-Carbajal *et al.* 2013; Brown *et al.* 2016; Salehinejad *et al.* 2017). MDE algorithms are able to determine several parameters where the number of parameters are higher than the population size. In the algorithm, MDE can solve more than 30 parameters with number of population from 5 to 8. Thus, in this paper, MDE is proposed for accurate and rapid determining of the best model parameter for single and multiple self-potential anomalies. Using MDE approach in the inversion, computation time for inversion process can be lessened.

2. Self-potential

The self-potential (SP) data for a simple polarized structure (figure 1a and b) at a point x_i can be represented as:

$$v(x_i) = K\frac{(x_i - D)\cos(\theta) + h\sin(\theta)}{\left((x_i - D)^2 + h^2\right)^q}, \qquad (1)$$

where K denotes the polarization amplitude (or electrical dipole moment), θ indicates the polarization angle, x_i describes a measurement point coordinate at the surface along the profile and h is the depth of the anomaly body's center source and D describes the anomaly located at the center from the origin of the measurement point, while q denotes the shape factor, which is equal to 1.5, 1.0, and 0.5 for sphere, horizontal cylinder, and semi-infinite vertical cylinder, respectively.

The SP anomaly is located at a point on the surface, on a line perpendicular to the strike of an inclined sheet of infinite horizontal extent (perpendicularly to the measuring profile, figure 1c), as given by the following (Biswas and Sharma 2014c):

$$v(x_i) = K\log\left(\frac{\{(x-D) - a\cos\theta\}^2 + (h - a\sin\theta)^2}{\{(x-D) + a\cos\theta\}^2 + (h + a\sin\theta)^2}\right), \qquad (2)$$

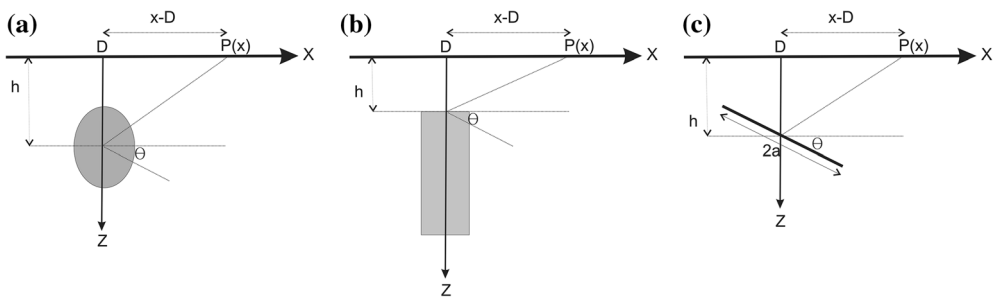

Figure 1. Description of model parameters for horizontal cylinder and sphere (**a**), vertical cylinder (**b**), and inclined sheet (**c**) in subsurface.

where θ denotes the inclination angle and a is the half-width of the sheet. The other notations have the same meaning as equation (1). Equation (2) has a property that a model is only geologically relevant if $h > a\sin\theta$ (Biswas and Sharma 2014b). This condition must be owned by inclined sheet model parameters.

Furthermore, the SP anomaly caused by multiple anomaly sources is obtained through the summation of responses due to individual anomalies (Biswas and Sharma 2014c). Mathematically, the multiple SP anomaly sources can be expressed as follows:

$$V(x_i) = \sum_{j=1}^{NM} v_j(x_i), \tag{3}$$

where $v_j(x_i)$ indicates the SP anomaly at x_i measured location for jth body and NM represents the number of bodies.

3. SP data inversion using micro-de algorithm

3.1 *Standard DE*

DE algorithm is generated by vectors (numbers of population) in the model spaces as candidate solutions. Further, DE attempts to improve the population for each generation to find an optimal solution using several processes in the DE algorithm. The population $P = \{X_1, \ldots, X_{Np}\}$ consists of number of population (Np) vectors in each generation, where each vector X_i contains the number of model parameter, generally called d dimension. Consequently, each X_i vector is defined as $X_i = (X_{i,1}, \ldots, X_{i,d})$. DE algorithm generally consists of the four processes including mutation, constrain handling, cross-over, and selection.

Meanwhile several approaches appear in the mutation process generally used in the standard DE as the following (Zhang and Sanderson 2009; Brown *et al.* 2016; Salehinejad *et al.* 2017):

(1) DE/rand/1

$$V_i = X_{i_1} + F(X_{i_2} - X_{i_3}), \tag{4}$$

(2) DE/current-to-best/1

$$V_i = X_i + F(X_{\text{best}} - X_i) + F(X_{i_1} - X_{i_2}), \tag{5}$$

(3) DE/best/1

$$V_i = X_i + F(X_{\text{best}} - X_1), \tag{6}$$

where the indices i_1, i_2, and i_3 represent different integers uniformly selected from the population such as $i_1 \neq i_2 \neq i_3 \neq i$ where $i \in \{1, \ldots, Np\}$, X_{best} indicates randomly selected individuals from the top 100% individuals in the current population with $p \in (0, 1]$, while F denotes the mutation factor, in which $F \in (0, 2]$. The exploration and exploitation of DE algorithm depends on that factor, where exploration can be decreased by selecting lower values for F.

After the mutation process, boundary handling is used to keep the model parameter values always within the model spaces. There are several boundary handling approaches, but in this paper boundary handling is represented as follows (Zhang and Sanderson 2009):

$$V_{i,j} = \begin{cases} (X_{i,j} + X\min_j)/2, & \text{if } V_{i,j} < X\min_j \\ (X_{i,j} + X\max_j)/2, & \text{if } V_{i,j} > X\max_j \\ V_{i,j}, & \text{otherwise,} \end{cases} \tag{7}$$

where $X\min_j$ and $X\max_j$ are the lower and upper bounds of X_j, respectively and $j = 1, \ldots, d$. Furthermore, cross-over process is applied in the DE through interaction between the mutant and parent vector:

$$U_{i,j} = \begin{cases} V_{i,j}, & \text{if } \text{rand}(0,1) \leq C_r \text{ or } j_{\text{rand}} = j \\ X_{i,j}, & \text{otherwise} \end{cases} \tag{8}$$

where C_r indicates the parameter of cross-over rates within the range of [0, 1]. The parameter controls how many components are mutated in each element from the mutant vector of the current population. The rand$(0, 1)$ represents a real random uniform number in the interval $[0, 1]$, while j_{rand} is a randomly selected integer in the range [1, d]. The binomial cross-over operator copies the jth parameter of the mutant vector $V_{i,j}$ to the corresponding element in the trial vector $U_{i,j}$, if rand$(0, 1) \leq C_r$ or $j_{\text{rand}} = j$. Moreover, it is copied from the corresponding target vector $X_{i,j}$.

The cross-over in DE is used to increase the population diversity. Furthermore, acquisitive selection is applied for selection in balancing exploration and exploitation capabilities of DE. Selection is carried out through comparison between the fitness value of U_i and X_i vectors where the one with better fitness value is elected for the next generation.

$$X_i = \begin{cases} U_i, & \text{if } f(U_i) \leq f(X_i) \\ X_i, & \text{otherwise.} \end{cases} \tag{8}$$

3.2 *Micro-DE approach*

MDE generally uses a very small population size compared to standard DE. Smaller population size means faster convergence rate. However, the solution is at risk of trapping in the local optimum. Therefore, in order to increase the diversity in population of MDE algorithm (Salehinejad *et al.* 2016, 2017) a slightly modified mutation factor in the standard DE is proposed, where vectored random mutation factor is used for every single dimension of each individual. Consequently, the algorithm is called MVDE. Therefore, the mutation factor is defined for each individual i as follows (Salehinejad *et al.* 2017):

$$F_i = \{F_{i,1}, \ldots, F_{i,d}\}, \qquad \forall_i \in \{1, \ldots, Np\}, \tag{9}$$

where $F_{i,j}$ is generated using random uniform distribution (Olguín-Carbajal *et al.* 2013; Salehinejad *et al.* 2017). C_r in the MVDE is set as in the standard DE. Further, MDE algorithm is started with an initial population. Then the mutation is estimated using equations (4–6), while boundary handling and cross-over steps are determined similar to the DE algorithm using equations (7) and (8), respectively. After the processes, greedy selection is applied to determine the population for the next generation. The termination condition is met when the maximum number of generations has been satisfied.

On the other hand, because the mutation factor is generated by a random value, the MDE results may be unstable and become trapped in the local optimum. Different from MVDE, Brown *et al.* (2016) proposed an adaptive MDE, called μJADE. In the algorithms, both mutation factor and cross-over rate parameters are adaptively determined for solving optimization problems with micro-population and external archive. The algorithm is modified from JADE to avoid a user's prior knowledge of the relationship between the parameter settings and the characteristics of the optimization problems. In the μJADE algorithm, modified DE/current-to-best/1 (equation 5) is used as the mutation operator, as following:

$$V_i = X_i + F_i(X_{\text{best}} - X_{i_1}) + F_i\big(X_{i_2} - \hat{X}_{i_3}\big), \tag{10}$$

where $\hat{X}_{i_3}$ is randomly selected from $P \cup A$, union of the current population and the archive, while F_i describes the mutation factor associated with X_i. In this paper, F_i is generated through adoption in JADE (see original paper) and updated for each iteration (Zhang and Sanderson 2009; Brown *et al.* 2016). Furthermore, the mutation operator in μJADE is equal to that in standard DE, but C_r is modified as the following

$$b_{i,j} = \begin{cases} 1, & \text{if } \text{rand}(0,1) \le C_r \text{ or } j_{\text{rand}} = j \\ 0, & \text{otherwise} \end{cases} \tag{11}$$

$$C_{ri} = \frac{\sum_{j=1}^{d} b_{i,j}}{d}. \tag{12}$$

Furthermore, perturbation mechanics are applied in order to correct the cross-over and $b_{i,j}$ results. The perturbation is described as follows:

$$U_{i,j} = \begin{cases} L_j + \text{rand}(0,1)\big(U_j - L_j\big), & \text{if } \text{rand}(0,1) \le 0.005 \\ U_{i,j}, & \text{otherwise} \end{cases} \tag{13}$$

$$b_{i,j} = \begin{cases} 0, & \text{if } \text{rand}(0,1) \le 0.005 \\ b_{i,j}, & \text{otherwise.} \end{cases} \tag{14}$$

After the mutation process, greedy selection approach is applied to select both further and archive population. When the best objective function does not improve for max(10,1d) generations, the population (excluding the best solution) is re-initialized.

3.3 *Inversion using MDE*

In order to invert SP anomaly using MDE algorithm, several SP parameters (as in equations 1 and 2) are accommodated in the X_i vector (equation 4). Using forward problem as equations (1) and (2) seems simple. However, the inversion of both problems in reality are very difficult to solve (Tlas and Asfahani 2013; Biswas and Sharma 2014b). Furthermore, the SP parameters are determined through MDE algorithm in a way to minimize the objective function Q, namely (Monteiro Santos 2010):

$$Q = \frac{2\big\| V_i^o - V_i^c \big\|}{\big\| V_i^o - V_i^c \big\| + \big\| V_i^o + V_i^c \big\|}, \tag{15}$$

where V_i^o and V_i^c describe the observed and calculated self-potential data, respectively. N denotes the number of observed self-potential data. Furthermore, the misfit between measured and inverted SP data is evaluated using the

average relative error (in %) and can be defined as:

$$\text{misfit}(\%) = \frac{100}{N}\sqrt{\sum_{i=1}^{N}\left(\frac{V_i^o - V_i^c}{V_i^o}\right)^2}. \qquad (16)$$

In general, GOMs as MDE have two properties namely, exploration and exploitation. Exploration in the DE variant is used to preserve diverse populations, while exploitation is used to choose the best candidate model parameters. Ideally, the two properties must balance out, because if the DE leans more towards exploitation, the algorithm will often become trapped in the local optimum, which can lead to fast convergence. Conversely, DE will find the true global optimum model slowly. Furthermore, when DE focuses in exploration, the solution of model parameters for DE with a balance between the two properties is fast convergence and the solution is around the true model parameter (optimum global).

An algorithm used to invert SP anomaly generally needs balancing exploitation and exploitation capabilities. The capabilities are crucial for the algorithms performance in order to estimate the posterior distribution model (PDM) of the SP anomaly. PDM works to handle non-unique solution in the inversion process (Sungkono and Santosa 2015). Generally, PDM can be provided by GOM with applied threshold for the objective function. The approach can be studied further in the following papers (Sungkono and Warnana 2018; Sungkono 2020).

4. Synthetic data

Before MDE is applied to field SP data, it is used to determine model parameters for mono-source SP anomaly. Specifically, in an inclined sheet model, as presented in table 1. Moreover, MDE is also tested in two anomaly sources of SP profile generated by two simple polarized anomalies as a sphere and horizontal cylinder, as listed in table 2.

4.1 *Parameter tuning of MDE*

Generally, performance of DE algorithm is controlled by three parameters including F, C_r and Np. The μJADE does not require C_r, F, and Np can be set to 8, while MVDE algorithm only depends on the C_r, because F is automatically generated and Np can be set to 5 (>4 as the minimum in 'DE/rand/1') for solving high dimension (10, 30, 50, and 100) (Olguín-Carbajal *et al.* 2013; Salehinejad *et al.* 2017). The condition is different to standard DE, where the minimum of Np required is $5d$–$10d$ (Yang 2014). This means that solving a model parameter with 30 dimensions requires 150–300 populations.

Furthermore, the adequate value of C_r in MVDE affects the convergence rate and it depends on the problem to be solved. For instance, $C_r \leq 0.2$ can be used for the separable functions, while $C_r \geq 0.9$ can be used for the non-separable ones (Ronkkonen *et al.* 2005). Consequently, several test performance in the inversion process using MVDE is acquired with several of $C_r \in [0.1, 0.9]$ in order to find global optimization and provide good PDM. However, in order to maintain populations diversity, the parameter of F is set as $F_{i,j} = \text{rand}[0.1, 1.5]$ (Olguín-Carbajal *et al.* 2013) and $F_{i,j} = \text{rand}[0, 1.5]$. Table 1 is the success rate (SR) (if the minimum objective function can be found under 0.05) and statistics of the MVDE objective functions with several C_r value and two ranges of F from 20 independent runs for noise-free SP synthetic data inversion (table 2). The inversion uses 5 populations and 800 generations (number of function evaluation/NFE set to 4000). Table 1 demonstrates that $F_{i,j} = \text{rand}[0.1, 1.5]$ with $C_r = 0.5$ has the highest SR and best objective function of inversion of SP anomaly. Thus, the parameters ($F_{i,j} = \text{rand}[0.1, 1.5]$ and $C_r = 0.5$) are clearly the best option in terms of the objective function statistics and therefore can be used to invert SP data. The change of mutation factor for the last parameter of each iteration in MVDE is presented in figure 2(a).

Furthermore, the MVDE results are compared with those of standard DE and μJADE. In order to equalize the comparison, the NFE of standard DE and μJADE are also set to 4000. Consequently, standard DE (DE) and μJADE have operated using 50 and 8 for Np and 80 and 500 for maximum generation, respectively. Standard DE in this paper uses DE/best/1 as the mutation process with $F = 0.5$ and $C_r = 0.9$ (Balkaya 2013; Ekinci *et al.* 2016; Balkaya *et al.* 2017), while μJADE has an adaptive mutation factor and cross-over rates are adaptively determined as in figure 2(b). However, μJADE requires p, which is set to 0.05.

Figure 3 is the comparison between three methods (standard DE, MVDE and μJADE) for finding the global optima in the inversion of SP data. The figure shows that μJADE is more

Table 1. *The performance MVDE for inversion of noise-free SP data with various C_r and two mutation factor intervals.*

		Objective function					
F	C_r	Min.	Max.	Median	Interquartile	SR	Times (s)
[0:1.5]	0.1	1.80E-02	3.94E-01	1.00E-01	9.66E-02	25.00%	23.76
	0.2	1.52E-02	1.82E-01	7.94E-02	4.29E-02	15.00%	23.77
	0.3	4.05E-03	3.60E-01	8.46E-02	5.41E-02	30.00%	24.24
	0.4	1.22E-02	3.74E-01	8.21E-02	1.40E-01	30.00%	24.38
	0.5	3.98E-03	3.79E-01	8.78E-02	2.77E-01	15.00%	24.42
	0.6	2.97E-03	3.75E-01	7.66E-02	6.57E-02	25.00%	21.62
	0.7	4.28E-03	4.22E-01	9.48E-02	7.06E-02	15.00%	21.29
	0.8	5.48E-03	4.58E-01	9.52E-02	3.01E-01	25.00%	21.44
	0.9	4.19E-03	5.78E-01	9.27E-02	1.93E-01	15.00%	**20.8**
[0.1:1.5]	0.1	2.12E-02	3.12E-01	9.67E-02	4.81E-02	10.00%	23.58
	0.2	1.67E-02	3.77E-01	8.66E-02	4.11E-02	10.00%	24.29
	0.3	1.45E-02	3.75E-01	7.70E-02	6.65E-02	35.00%	24.26
	0.4	2.46E-03	3.84E-01	4.99E-02	8.10E-02	50.00%	24.81
	0.5	**3.56E-05**	**3.59E-01**	**4.05E-02**	**8.15E-02**	**60.00%**	24.47
	0.6	1.24E-04	2.32E-01	7.53E-02	6.27E-02	35.00%	24.98
	0.7	6.28E-03	3.75E-01	9.17E-02	2.71E-01	10.00%	24.34
	0.8	2.28E-03	4.87E-01	9.13E-02	2.61E-01	15.00%	25
	0.9	1.62E-04	4.16E-01	2.78E-01	2.85E-01	20.00%	24.56
μJADE		**2.25E-12**	**9.47E-02**	**1.47E-06**	**2.87E-02**	**80.00%**	**22.32**
Standard DE		1.35E-02	9.46E-02	8.15E-02	3.73E-02	0.00%	25.82

NFE is set 4000 for all algorithms (standard DE, MVDE, and μJADE) and various parameters of MVDE. The optimum of SR (success rates) for MVDE is denoted by bold face, i.e., using parameter of DE $F_{i,j} = \text{rand}[0.1, 1.5]$ and $C_r = 0.5$. Standard DE uses 0.9 and 0.5 for F and C_r, respectively, while μJADE is adaptive to determine both parameters. However, the best accelerates the convergence speed is μJADE (figure 3) if the performance of MVDE, μJADE and standard DE are compared.

efficient and more robust for determining model parameters in SP data inversion comparison to MVDE and standard DE, because μJADE is capable of finding the global optimum around 2500 of NFE, while the others fail to seek until the last NFE. Furthermore, μJADE, MVDE and standard DE have 80%, 60% and 0% of SR (table 1). The time consumed by the three algorithms (DE, MVDE and μJADE) are comparable (table 1), because NFE is set as the same for all algorithms.

4.2 *Inversion of single anomaly*

Figure 4 shows synthetic noise-free and noise-added (dots) of SP anomaly parameter with inclined sheet sources (table 2). As described above, MDE (MVDE and μJADE) has probably failed to search for model parameter in SP data inversion. Consequently, MDEs are processed using a minimum of five independent runs (except for noise-free data) for obtaining good PDM. The model response (table 2) from the best objective function of five independent runs is depicted through synthetic SP data in figure 4(a–d). The calculated data of the MDE (MVDE and μJADE) shows relatively good fitting for 'observed' SP data.

Figure 5 shows the best objective function for each iteration of both MVDE and μJADE algorithms of several noise levels. The figure indicates that noise in SP data can deform the objective function in the inversion process, where this result is supported by several researchers (Fernández-Martínez *et al.* 2014a, b). Moreover, figure 5 also demonstrates that μJADE and MVDE algorithms can reach convergence at around 2000–3500 and 2000–3800 of NFE, respectively. The convergence curves use to determine threshold for generating PDM.

In order to handle non-unique solution of SP data inversion, PDM is revealed from the threshold of objective function of the best MDE results. The threshold values for providing the PDM are 0.05, 0.075, 0.1, and 0.13 for noise-free data and Gaussian noise-added with 5%, 10% and 15%, respectively. The PDM results are based on the threshold value (Vrugt and Beven 2018), while the strategy in determining the threshold is clearly described in the papers (Sungkono and Warnana 2018;

Table 2. *Synthetic model parameters, parameter ranges using MDE (MVDE and μJADE) inversion, and corresponded results for an inclined sheet model synthetic with noise added levels variation and their inversed model parameter using MDE.*

			Comparison MVDE and μJADE for different level of noises in the SP data							
			Noise-free		5% noise		10% noise		15% noise	
Parameters	Ranges	True models	MVDE	μJADE	MVDE	μJADE	MVDE	μJADE	MVDE	μJADE
K (mVm)	−1000:1000	50	49.99 ± 0.00	50.00 ± 0.00	53.30 ± 0.04	53.26 ± 0.01	59.08 ± 1.43	49.18 ± 1.17	72.94 ± 18.90	63.72 ± 0.08
D (m)	0:100	55	55.00 ± 0.00	55.00 ± 0.00	54.62 ± 0.01	54.62 ± 0.00	53.64 ± 0.06	55.20 ± 0.34	53.61 ± 1.66	54.04 ± 0.00
a (m)	1:40	10	10.00 ± 0.00	10.00 ± 0.00	10.14 ± 0.01	10.14 ± 0.00	10.22 ± 0.03	9.83 ± 0.11	4.22 ± 1.17	10.71 ± 0.01
θ (°)	0:180	150	150.00 ± 0.00	150.00 ± 0.00	149.11 ± 0.02	149.12 ± 0.00	147.10 ± 0.05	149.59 ± 0.74	123.78 ± 9.52	149.18 ± 0.00
h (m)	0:80	12	12.00 ± 0.00	12.00 ± 0.00	11.53 ± 0.00	11.54 ± 0.00	10.18 ± 0.23	12.28 ± 0.31	13.15 ± 1.38	9.60 ± 0.01
Minimum of the objective function			3.56E-05	2.25E-12	4.29E-02	4.29E-02	7.95E-02	7.33E-02	1.19E-01	1.06E-01
Maximum of the objective function			3.59E-01	9.47E-02	3.68E-01	4.30E-02	1.20E-01	3.09E-01	3.72E-01	1.17E-01
Median of the objective function			4.05E-02	1.47E-06	5.84E-02	4.29E-02	1.19E-01	7.33E-02	1.19E-01	1.07E-01
Interquartile of the objective function			8.15E-02	2.87E-02	1.18E-01	1.07E-05	2.01E-02	8.22E-02	1.25E-01	3.90E-03

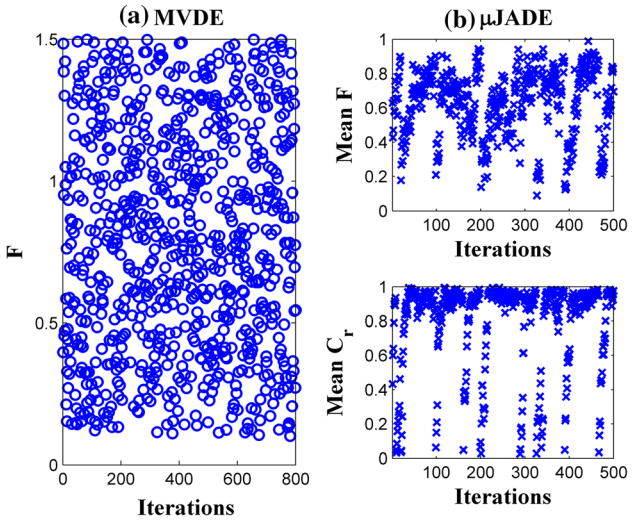

Figure 2. Changes of mutation factor and cross-over rates of MDE variants for inversion noise-free of SP data; (**a**) changed mutation factor for the last parameter in MVDE algorithm; and (**b**) changed mutation factor (upper panel) and cross-over rates (lower panel) for μJADE algorithm.

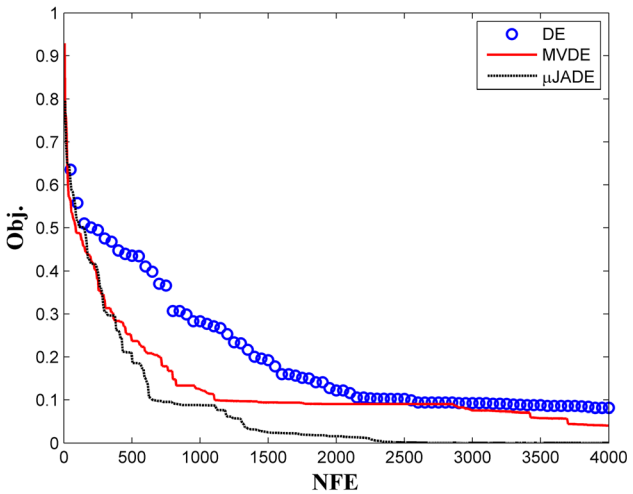

Figure 3. Comparison of the best objective function for MDE (MVDE and μJADE) and standard DE in inversion of SP data. The mutation factor and cross-over rates are set as table 1 (the bold face type for MVDE), 0.9 and 0.5, respectively, for standard DE, and is adaptively set for μJADE. The μJADE algorithm indicates faster and more robust than others.

Sungkono 2020). The best curve fitting acquired from inversion using both algorithms are presented in figure 4, while the statistical values of PDM are presented in table 2. The median of PDM describes the best model parameter, while the interquartile of PDM reflects the uncertainty of model parameters. The estimated model parameters indicate that the higher noise in the data can be shifted out of the inversion result and objective function (table 2) (Pallero *et al.* 2015).

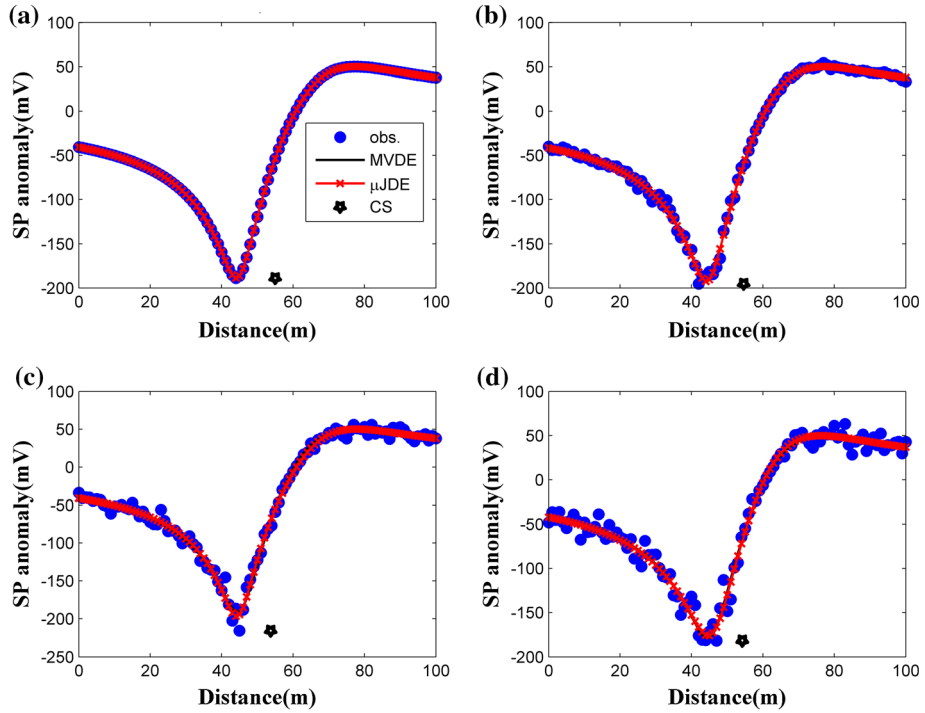

Figure 4. Synthetic data for an inclined sheet contaminated without and with 5%, 10%, and 15% Gaussian noise with their inversion results (**a**), (**b**), (**c**), (**d**), respectively. Dots indicate the synthetic data, while the solid line shows the response model parameter resulted by MDE variants (MVDE and μJADE). Solid lined indicates MVDE, while line crosses denotes μJADE.

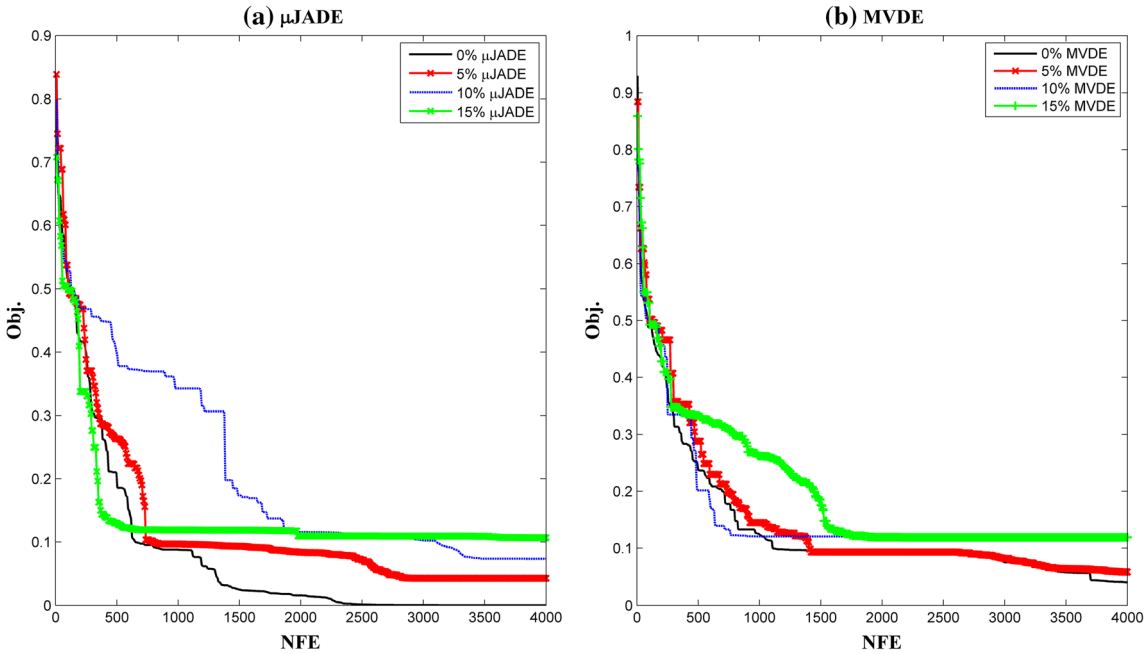

Figure 5. Median of the best objective function (Obj) resulted by MDE as function of the NFE for various noises containing in the SP data; (**a**) μJADE; (**b**) MVDE. The median is created by 20 independent runs for noise-free synthetic data, while others derived by 5 independent runs.

Furthermore, the PDM histogram as revealed by noise-free SP data inversion using μJADE (upper panel) and MVDE (lower panel) are demonstrated in figure 6. The figure indicates that the high probability of PDM is correlated to its median and true model parameters. This means that both

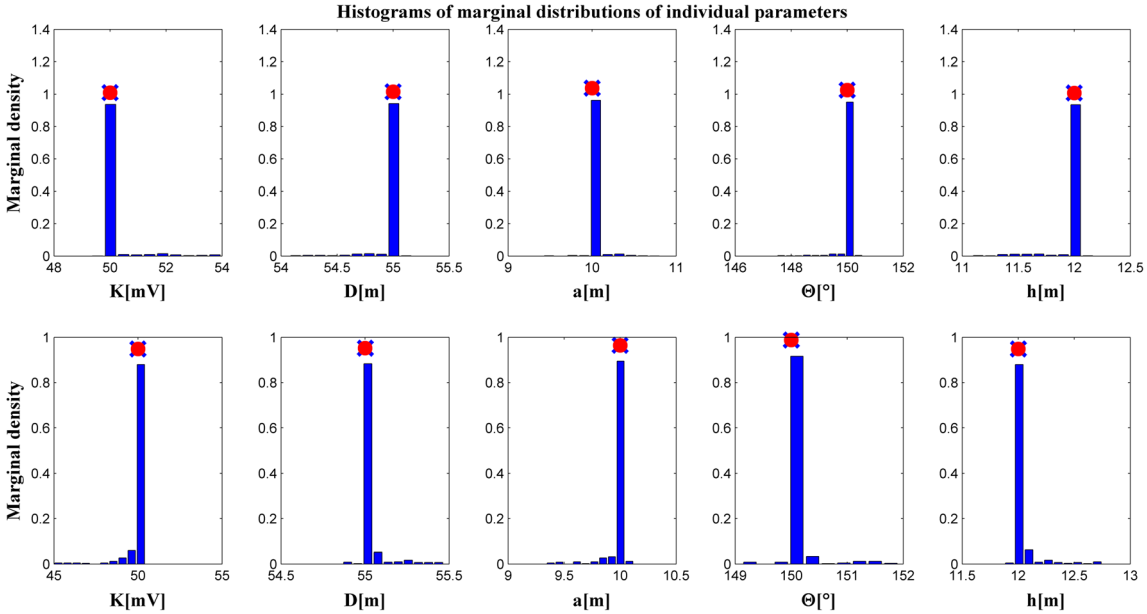

Figure 6. Histogram of DPM for each parameter of noise-free SP data revealed by μJADE (upper panel) and MVDE (lower panel). Both panels indicate that higher probability of PDM correlates with true model parameter (dots) and median of PDM (crosses). It means that both algorithms are able to determine PDM.

algorithms are able to provide PDM in SP inversion. Furthermore, the process is repeated to generate PDM in future sections.

4.3 *Inversion of multiple anomalies*

SP anomaly generally contains more than one source. In deriving model parameter of two-source anomalies (10 model parameters), MVDE and μJADE use 7000 of NFE for inverting the synthetic data, where both MVDE and μJADE utilize 7 and 8 populations, respectively. It means that the size of model parameters is greater than the size of the populations, where such condition cannot be applied in standard DE. In addition, for inversion of two-source anomalies MDE (MVDE and μJADE) only needs 7000 forward computations, where the amount is ultimately slightly less when compared to the needs of the whale optimization algorithm (WOA) (Abdelazeem *et al.* 2019) and black holes algorithm (BHA) (Sungkono and Warnana 2018) that require 200,000 and more than 140,000, respectively. It indicates that the MDE (MVDE and μJADE) is far more capable than WOA and BHA in the forward calculation.

Furthermore, the synthetic and the calculated SP data are shown in figure 7(a), while the true model parameters and the parameters ranges for the inversion process are tabulated in table 3. The inversion is processed 10 independent times to overcome the premature result of the inversion.

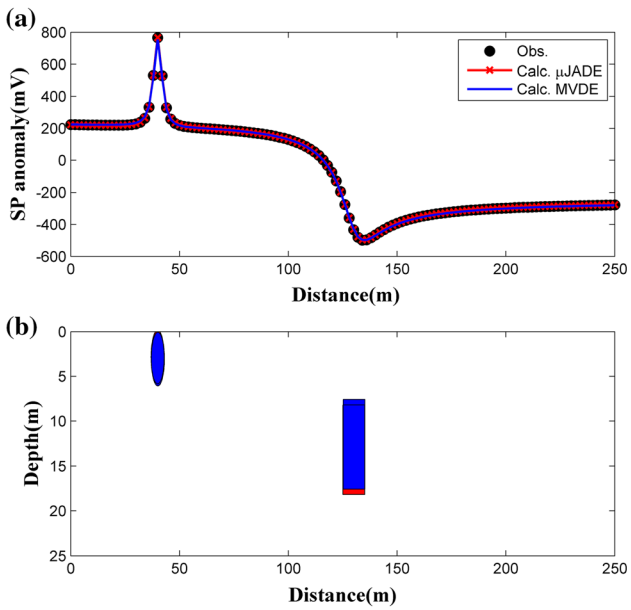

Figure 7. Synthetic data and two sources of idealized bodies and its model response of inversion results. (**a**) Black dots indicate the synthetic data, solid line is model response of MVDE result and solid crosses line represents μJADE result, (**b**) The sketches is representing the model parameter revealed by MVDE (blue) and μJADE (red) inversion for synthetic data anomaly. The positions of anomalies are identic for both algorithms.

From 10 processes, one process is selected based on the lowest objective function. After that, PDM is determined using limit acceptability (described before) from selection process. Furthermore, median of the PDM reflects the model parameter

Table 3. *Synthetic model parameters, parameter ranges in MDE variants inversion, and their results for the two synthetic models (sphere and vertical cylinder) and inversed model parameters.*

Parameters	Sources	K (mVm)	D (m)	h (m)	θ (°)	q
Ranges	1	3000:7000	20:60	0:50	0:180	0.01:2
	2	−1000:0	80:200	0:50	0:180	0.01:2
True Parameters	1	5000	40	3	90	1.5
	2	−500	130	8	60	0.5
MVDE	1	3190.32 ± 551.78	40.03 ± 0.38	3.06 ± 0.51	91.75 ± 12.32	1.32 ± 0.05
	2	−501.96 ± 38.55	130.26 ± 0.51	7.58 ± 0.64	60.67 ± 2.26	0.50 ± 0.02
μJADE	1	3383.72 ± 73.16	39.95 ± 0.04	2.83 ± 0.01	88.06 ± 2.14	1.37 ± 0.01
	2	−502.81 ± 64.81	130.12 ± 0.36	8.19 ± 0.01	60.05 ± 2.21	0.5 ± 0.03

solution, while the interquartile indicates the uncertainty model parameter to handle non-unique model solutions in the inversion (Sungkono and Santosa 2015). The median of PDM resulted by MVDE and μJADE is similar to the true model parameters (except amplitude of polarization and shape factor for fist anomaly, as presented in table 3. Furthermore, figure 7(a) indicates a good-fit between the observed and calculated models from MVDE and μJADE, while figure 7(b) shows that the position and shape of anomalies from both algorithms are similar.

5. Field studies

MDE variants performance is examined through different field SP anomaly optimization problems. The field SP anomalies are classified into two distinct types, single and multiple anomaly sources. Multiple sources are generally measured in SP profiles because of the complexity and variety of mechanisms that can affect SP data such as geological and topographical conditions. In this section, the MDE results are given in seven examples of SP field data that represent single and multiple SP anomalies including Sawoo, Pinggirsari, and LUSI embankment anomalies (Indonesia), Neemka-Thana anomaly (India), KTB anomaly (Germany), and Karakoç creek (Turkey). Moreover, these examples will also be presented and compared with other approaches.

5.1 *Sawoo anomaly, Indonesia*

The SP survey that discovers the anomaly was measured in the landslide potential area, Sawoo district, Ponorogo regency, East Java, Indonesia. The SP data is corroborated after the regional effects has been removed. The anomaly is used to identify the position and depth of fluid accumulation which is caused by landslides. Sungkono and Warnana (2018) have analyzed the anomaly using BHA, while Ramadhani and Sungkono (2019) have employed the anomaly using hybrid dragonfly algorithm with regressive–regressive PSO (MHDA), and Sungkono (2020) applied flower pollination algorithm (FPA) to derive the PDM of the data. Furthermore, in this example, the SP data is inverted using MVDE and μJADE approaches with 5 and 8 populations, respectively. Both algorithm processes use 5000 NFE for 10 independent runs. The PDM of both algorithms are set using 0.13 as the threshold of objective function.

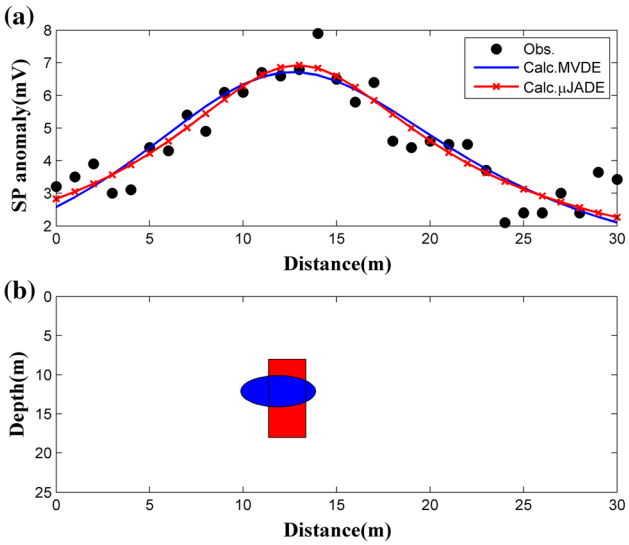

Figure 8. MDE inversion results for Sawoo anomaly (Sungkono and Warnana 2018); (**a**) comparison between observed (dots) and calculated SP anomaly using MVDE (solid line) and μJADE (crosses solid line), (**b**) subsurface model parameters revealed by MVDE (blue) and μJADE (red).

Figure 8(a) shows that the SP data calculated using MVDE and μJADE is similar to the observed data. The best model parameters and its

Table 4. *Parameter ranges used in MDE variants for Sawoo anomaly inversion and comparison of inversion results with BHA.*

Parameters	K (mVm)	D (m)	h (m)	θ (°)	q
Ranges	−1000:1000	00:30	0:100	0:180	0.1:1.9
BHA (Sungkono and Warnana 2018)	163.39 ± 75.80	12.01 ± 0.62	11.93 ± 0.85	82.07 ± 4.36	1.14 ± 0.10
FPA (Sungkono 2020)	504.99 ± 315.01	12.94 ± 2.35	15.64 ± 3.32	91.04 ± 2.19	1.29 ± 0.12
MHDA (Ramadhani and Sungkono 2019)	4.90 ± 0.15	13.03 ± 0.01	3.39 ± 0.08	90.74 ± 0.08	0.34 ± 0.00
MVDE	180.29 ± 2.37	11.87 ± 0.04	12.09 ± 0.20	81.17 ± 0.37	1.16 ± 0.00
μJADE	13.99 ± 2.45	12.36 ± 0.36	8.01 ± 0.43	86.60 ± 1.75	0.67 ± 0.04

uncertainty resulted by MVDE and μJADE is presented in table 4, and the result is compared with BHA, MHDA and FPA results. The uncertainty of FPA is higher than the others, meaning that FPA has explorative capacity in this inversion. The MVDE and μJADE results are interpreted in figure 8(b). The MVDE, BHA and FPA results indicate that the model parameters from all algorithms are very similar, where the anomaly source in the form of horizontal cylinder or pipe represents a fluid channel. The channel works to move fluid from the source zone to the accumulation zone.

On the other hand, the distance and polarization angle of all algorithms are similar, although polarization amplitude, depth and shape factor for both μJADE and MHDA are different to the others. The shape factor for μJADE and MHDA indicates a vertical cylinder at the near surface. The anomaly is located in the landslide scarf which is measured in the rainy season (Ramadhany *et al.* 2018). Consequently, in order to clearly understand the anomaly, other geophysical methods are needed.

Furthermore, the effectiveness of MVDE, μJADE, FPA and BHA is also compared in order to generate the model parameters. MDE variants, FPA and BHA need 500, 2000 and 6000 forward calculations, consecutively. From these numbers, it can be concluded that MDE variant (MVDE and μJADE) is more effective than BHA and FPA.

5.2 *Pinggirsari anomaly, Indonesia*

The SP survey anomaly was carried out in Pinggirsari village, West Java, Indonesia, on May 24, 2016, hence the name Pinggirsari anomaly. This anomaly was measured by crossing the fault, where the profile length has a separation of 10 m between each measuring electrodes. The SP anomaly is used to test the performance of MDE compared to whale optimization algorithm (WOA) (Gobashy *et al.* 2019) and Lavenberg–Marquardt algorithm (LMA) (Fajriani Srigutomo and Pratomo 2017).

In order to provide PDM, Pinggirsari anomaly is inverted using MVDE and μJADE with 1000 of NFE. As described above, MVDE and μJADE apply 5 and 8 populations, respectively. Because the Pinggirsari anomaly contains only one anomaly source and the MDE solution unlikely to be trapped in the local optimal, the MDE variant algorithm is set to 10 process times, but the result is not different from the minimum objective function. The best objective function as NFE for MVDE and μJADE is presented in figure 9(c). The figure shows that the MDE needs 250 and 450 of NFE in μJADE and MVDE, respectively, for reaching convergence and finding the global optima. This means that the convergence of μJADE and MDE involves 250 and 450 evaluation numbers, respectively, while in contrast, WOA involves 1700 evaluation numbers (Gobashy *et al.* 2019). Consequently, μJADE and MVDE are 68 and 37 times less in the calculation of evaluations (forward modelling and objective function). The condition shows that MVDE is faster and more effective for SP anomaly inversion compared to WOA.

Figure 9(a) demonstrates the comparison between calculated and observed SP anomaly from the Pinggirsari area. Furthermore, the MVDE and μJADE model parameters were compared with those revealed by WOA (Gobashy *et al.* 2019) and LMA (Fajriani Srigutomo and Pratomo 2017) algorithms as in table 6, which are presented in figure 9(b). It also show that the model parameter of MVDE and μJADE match each other. Furthermore, table 5 describes how the four approaches present that the shallow fault is identified and reinforced by narrow width as a property of the SP anomaly. In addition, the model parameters, except for the angle of the inclined sheet revealed by the three methods are very similar.

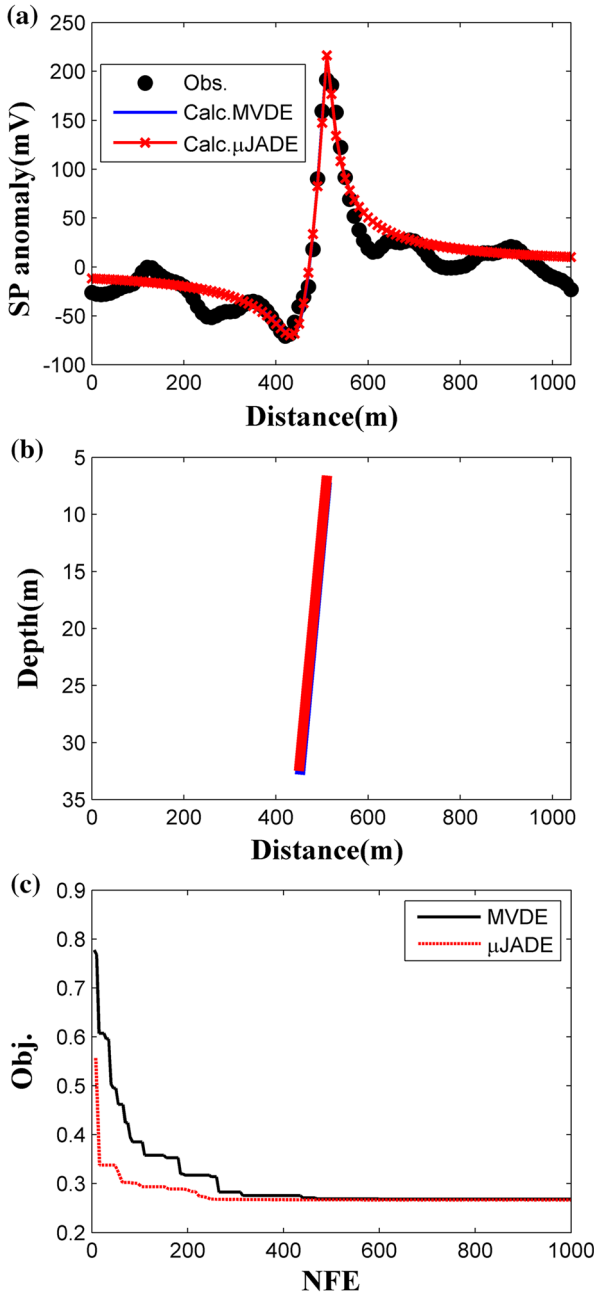

Figure 9. Pinggirsari anomaly result is analyzed using MDE (Fajriani Srigutomo and Pratomo 2017); (**a**) measured (dots) and calculated SP data using MVDE (black) and μJADE (red); (**b**) subsurface model parameters estimated by MVDE (blue) and μJADE (red), and (**c**) objective function *vs.* the NFE of both algorithms. The model of MVDE and μJADE are similar or identic.

5.3 *Neem-ka-Thana anomaly, India*

The SP survey anomaly measured in the Neem-Ka-Thana Copper Belt, India features copper mineralization as a SP anomaly source (Reddi *et al.* 1982). Copper mineralization is mostly located in the faults and shear planes. The copper concentrate in the mine varies from 0.6 to 1.2% (Biswas 2017). The SP anomaly has been analyzed by previous authors (Göktürkler and Balkaya 2012; Balkaya 2013; Biswas 2017) over the assumption that the SP anomaly contains a main source (simple polarized structure) using SA and their variant (very fast SA), GA, PSO, and DE. Using the same assumption, 2000 forward calculations are applied in MVDE and μJADE for determining model parameters (K, D, h, θ, q) simultaneously. As described above, both MVDE and μJADE algorithms require 5 and 8 populations, respectively. The result is presented in table 6. Figure 10(a) demonstrates the comparison between the observed data and the responses' model parameters. The resulting model parameters of MDE variants result are similar to the others. In addition, all approaches indicate that the main anomaly as a vertical cylinder which is presented in figure 10(b).

Furthermore, the SP anomaly presents three peaks, where there are two peaks before the main (third negative) anomaly. The Neem-ka-Thana anomaly has been interpreted using VFSA with three source models (Biswas 2017). Again, to identify the robustness of MDE variants including MVDE and μJADE algorithms, the algorithm is processed to invert the model parameter of the three sources idealized bodies. Figure 10(c) validates the comparison between calculated SP data revealed in MDE inversion and observed data with three sources idealized bodies, while table 7 is a comparison between MDE and VFSA results' model parameters. The table indicates that the position and depth of the three sources' models of both algorithms are alike. The shape factor of both

Table 5. *Parameter ranges used in the MDE variants inversion of Pinggirsari anomaly and comparison of MDE variants results with parameters revealed by WOA and GN.*

Methods	K (mVm)	D (m)	a (m)	θ (°)	h (m)
Ranges	10:60	400:600	20:60	−200:0	0:20
LM (Fajriani Srigutomo and Pratomo 2017)	41.5	478.25	34	334.52	14.63
WOA (Gobashy *et al.* 2019)	47.38	479.625	35.85	−149.98	15.68
MVDE	48.67 ± 1.00	481.01 ± 0.54	31.72 ± 0.78	−156.20 ± 0.30	20.00 ± 0.00
μJADE	46.85 ± 0.44	480.07 ± 0.09	33.01 ± 0.17	−156.93 ± 0.54	19.55 ± 0.72

Table 6. *Parameter ranges used in the MDE variants inversion of Neem-ka-Thana anomaly and comparison of MDE variants results with parameters revealed by others using source assumption.*

Model Parameters	Search space	VFSA (Biswas 2017)	Balkaya (2003)	Göktürkler and Balkaya (2012)			MDE	μJADE
				GA	PSO	SA		
K (mVm)	−100: 0	−32.2 ± 0.6	−48.50	−53.99	−49.53	−44.62	−48.38 ± 5.07	−49.93 ± 24.79
D (m)	150:200	177.8 ± 0.2	176.8	176.84	176.77	176.92	178.32 ± 2.68	176.66 ± 0.33
h (m)	00:50	10.8 ± 0.6	17.3	18.6	17.6	16.34	18.81 ± 1.31	17.91 ± 4.35
θ (°)	0:180	89.6 ± 0.1	88.05	87.83	88	88.25	88.95 ± 1.65	88.06 ± 0.76
q	0:2	0.5	0.4	0.42	0.4	0.38	0.41 ± 0.02	0.41 ± 0.08

Table 7. *Parameter ranges used in the MDE variants inversion of Neem-ka-Thana anomaly and comparison model parameters revealed by MDE variants and others using three sources assumption.*

Methods	Sources	K (mVm)	D (m)	h (m)	θ (°)	q
Search spaces	1	−100:0	50:100	0:50	0:180	0:2
	2	−200:0	100:150	0:50	0:180	0:2
	3	−300:0	150:200	0:50	0:180	0:2
VFSA (Biswas 2017)	1	−28.5	69.20	18.80	88.40	0.50
	2	−140.0	138.10	10.20	87.90	1.00
	3	−81.4	174.60	16.40	82.40	0.50
MVDE	1	−77.81 ± 16.13	82.70 ± 4,24	8.90 ± 1.75	147.88 ± 27.02	0.89 ± 0.02
	2	−98.55 ± 110.38	137.92 ± 24.92	23.38 ± 41.39	129.11 ± 52.29	1.5 ± 0.48
	3	−33.41 ± 2.25	176.40 ± 0.43	14.21 ± 0.74	88.70 ± 0.04	0.32 ± 0.01
μJADE	1	−100 ± 0.00	81.03 ± 0.56	16.23 ± 2.09	126.16 ± 2.51	0.77 ± 0.02
	2	−199.4 ± 1.83	145.62 ± 1.09	7.56 ± 0.18	179.99 ± 0.03	1.092 ± 0.03
	3	−164.40 ± 2.90	172.21 ± 0.47	28.14 ± 1.30	81.55 ± 1.06	0.59 ± 0.00

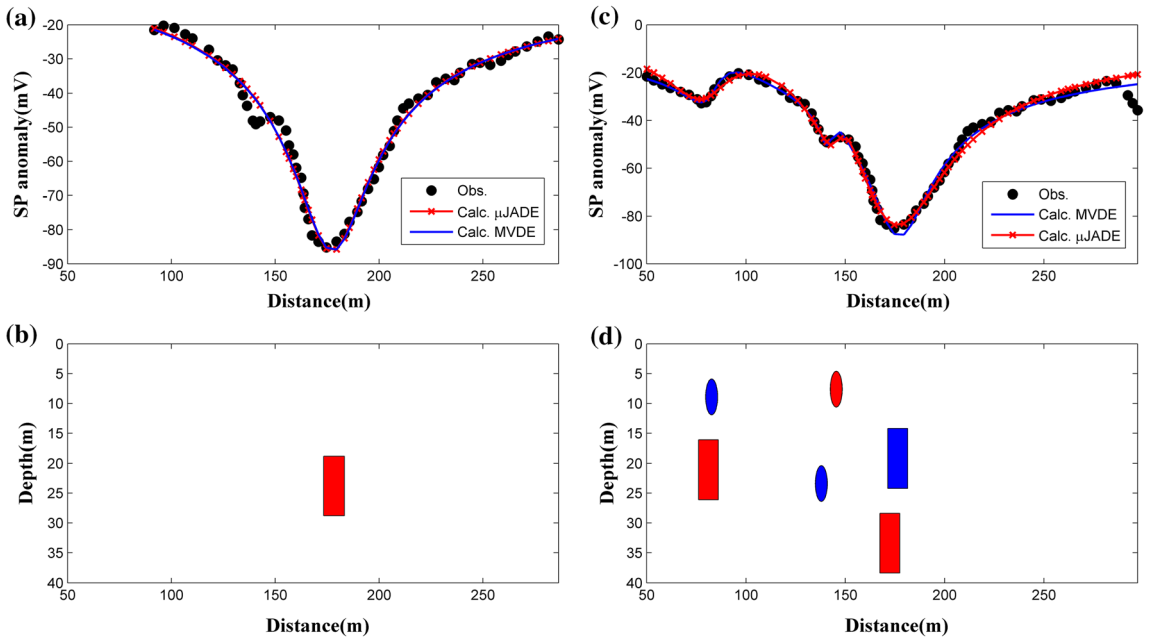

Figure 10. MDE inversion results for Neem-ka-Thana anomaly; (**a**) comparison between observed (dots) and calculated (solid line) of SP anomaly using assumption as a source idealized body; (**b**) subsurface model parameters for a source of idealized body using MVDE (blue) and μJADE (red); (**c**) comparison between observed (dots) and calculated SP anomaly using assumption three sources of idealized bodies for MVDE (solid line) and μJADE (crosses solid line); and (**d**) subsurface model parameters for three sources idealized bodies.

MDE and μJADE formed results showed as vertical cylinder for the last anomaly, in agreement with Biswas (2017). This also happened in the second anomaly. However, the shape factor for the first anomaly of both MVDE and VFSA is different, but type anomaly of VFSA for the first anomaly is possibly similar with μJADE results, where the algorithms interpreted the shapes as horizontal and vertical cylinders, respectively. Furthermore, the electrical dipole moment and polarization phase for the first and second anomaly in the both algorithms are quite different. The difference might be caused by self-potential ambiguity and negative correlation between the electrical dipole moment and polarization angle (Biswas and Sharma 2015).

Tables 6, 7, and figure 10(b and d) show that the main anomaly resulted by MDE variants are a semi-infinite vertical cylinder. The results are also supported by other algorithms (tables 6 and 7). However, in the present work, the Neem-ka-Thana anomaly in the main anomaly was also analyzed using standard DE with more than 5226 evaluation number (Balkaya 2013), while using MDE variants only requires 2000 forward computation. Furthermore, in order to interpret the multiple anomalies, MDE variants require 10,000 evaluation numbers, while VFSA requires 1 billion forward computations (Biswas 2017). Last but not least, MDE is more effective than VFSA for inverting SP data in the forward computations.

5.4 *LUSI embankment anomaly, Indonesia*

LUSI embankment protects the residential area from a local mud eruption in the Sidoarjo district, East Java, Indonesia. Assessment of LUSI embankment is acquired using several geophysical techniques such as Rayleigh wave dispersion, resistivity, and very low frequency methods (Sungkono *et al.* 2018). In addition, Husein *et al.* (2014) used ground penetrating radar to identify subsidence (vertical deformation) and crack in the embankment. Stability of the embankment is distressed by deformation, which are two faults through the embankment, fluid seepage, etc. (Sungkono *et al.* 2014, 2018).

SP data in the LUSI embankment has been interpreted using several approach including BHA (Sungkono and Warnana 2018) and WOA (Abdelazeem *et al.* 2019). Sungkono and Warnana (2018) consider the SP data to contain four sources with different positions. The efficiency and robustness of MDE variants are evaluated by analyzing SP data in the LUSI embankment anomaly with four sources (20 parameters) using 5 and 8 populations for MVDE and μJADE algorithms, respectively, where the process for both algorithms is set to stop when the NFE reaches 3000. It means that the algorithm can be used to determine the number of parameters which are higher than the MDE population. The anomaly has been analyzed and computed using 20 parameters from BHA (Sungkono and Warnana 2018), WOA (Abdelazeem *et al.* 2019) and FPA (Sungkono 2020). The algorithms are processed using 10 independent runs to provide PDM. Several model parameters with objective function below 0.2 are utilized as PDM candidate.

Figure 13 shows a comparison between the MVDE and μJADE results calculated from the parameters (table 10) and observed the SP anomaly. Table 10 shows a comparison between MDE variants and other methods, which demonstrate that entire anomaly parameters (except polarization magnitudes) from MDE variants are in good agreement with those found using BHA and WOA. Furthermore, entire algorithms discovered that the shape factors of the four anomalies are approximately equal to one, which represent horizontal cylindrical structures as sources at the different depths and distances. The horizontal structures are expected to be lateral cracking in the embankment body, which are specifically sourced from anomalies number 1 and 2.

Moreover, the efficiency of several algorithms (MDE variants, WOA, and BHA) are evaluated in terms of forward modelling calculation numbers. MVDE, μJADE, WOA and BHA each require 15,000, 24,000, 120,000, and more than 300,000 times for the calculation of both forward modelling and objective function, respectively. This indicates that the MDE variants are 5–12.5 times faster than others, yet with similar results (table 10).

5.5 *KTB anomaly, Germany*

Figures 11 and 12 show the KTB anomaly field (marked with dots) which was observed near the KTB-boreholes, drilled during the German Continental Deep Drilling Program (Stoll *et al.* 1995). The anomaly contains two negative peak anomalies at different amplitudes (–400 and –600 mV) produced by graphitic shear zones, which identify the position of the subsurface structure model. The SP

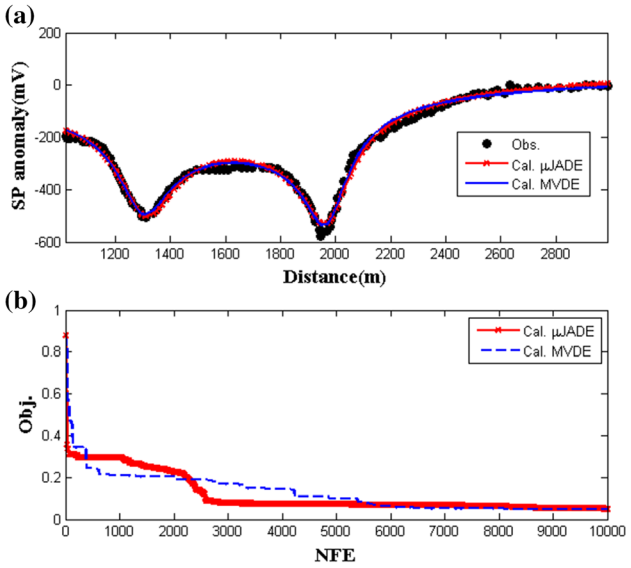

Figure 11. Field SP data from the KTB anomaly (Stoll *et al.* 1995), Germany, inversed using MDE with the sources derived by two sources of idealized bodies; (**a**) field data (dots) and model response represents solid line and cross solid line for MVDE and μJADE, (**b**) objective function with NFE.

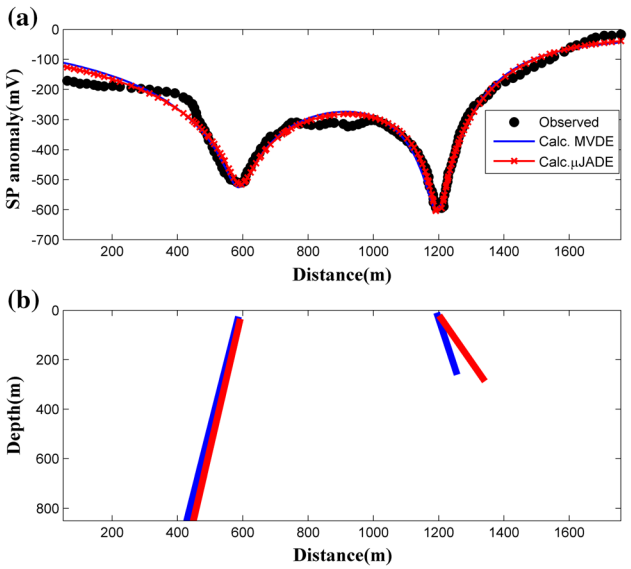

Figure 12. Field SP data from the KTB anomaly (Stoll *et al.* 1995), Germany, inversed using MVDE and μJADE with the sources derived by inclined sheet; (**a**) field data represents dots, while model response of MVDE and μJADE indicates solid line and crosses solid line, respectively; (**b**) subsurface structure for multiple bodies revealed by MVDE (red) and μJADE (blue).

data was analyzed using two assumptions which are simple polarized and inclined sheet using several approaches as in tables 8 and 9, respectively. In order to compare with previous approaches, data has been digitized from Biswas (2017) and Di Maio *et al.* (2019) for inclined sheet and simple polarized assumptions, respectively. The anomaly is then simultaneously processed using MDE variants. In this inversion, the population numbers 5 and 7 are used on MVDE for simple polarized and inclined sheet model assumption, respectively, while 8 populations are applied for both assumptions in μJADE algorithm. Both algorithms are processed using 10,000 and 10,500 of NFE for simple polarized and inclined sheet models, respectively.

MDE variants are processed to invert the KTB anomaly with simple polarized and inclined sheet model. In each algorithm, 10 independent process runs are used to reveal the subsurface model in accordance with the geological study and reliable model parameter (especially for the inclined sheet model). The selected model parameter is not only based on the best objective functions (the inversion results from several process times correlated to the lowest objective is selected to be applied as the threshold for the objective to provide PDM), but also based on the geological condition.

Figure 8 presents the comparison between observed and calculated data of MVDE and μJADE inversion using simple polarized assumption. The figure explains that the calculated data fits well with the field data from MDE results (table 8). In table 8, the model parameters and their uncertainty resulted by MDE variants is compared with other algorithms including GPA (Di Maio *et al.* 2019) and Gauss Newton algorithm (GNA) (Mehanee 2015). The model parameter results of μJADE are comparable with other approaches (table 8). Furthermore, MVDE results are similar to other algorithms' outputs especially for distance, polarized angle, and shape factor, whereas other parameters are dissimilar, which is caused by SP model properties (Biswas and Sharma 2015). As noted, the difference in negative signs between GPA and other approaches is caused by a different sign in the depth of equation (1). Based on the shape factor resulted through inversion using several approaches, it can be recognized that two sources represent the responsible structure (a fault). Consequently, several authors (Biswas 2017; Gobashy *et al.* 2019) applied inclined sheet in the inversion process.

In addition, for the second source MDE algorithm generates lower depth (h) and electrical dipole moment (K) values than those revealed using other methods. It is mainly caused by the dipole moment that has a positive correlation with depth (Biswas and Sharma 2015). Hence, if K

Table 8. *Parameter ranges used in the MDE variants inversion of KTB anomaly and comparison model parameters estimated by MDE variants and others using simple polarized as source.*

Methods	Sources	K (mVm)	D (m)	h (m)	θ (°)	q
Search spaces	1	200:9000	1100:1500	1:200	−30:180	0.01:2
	2	200:9000	1400:3000	1:200	−30:180	0.01:2
GNA (Mehanee 2015)	1	484.00	–	134.00	−99	0.50
	2	517.00	–	119.00	−79	0.50
GPA (Di Miao *et al.* 2019)	1	4669.00	1305.00	145.00	96.00	0.75
	2	1664.00	1967.00	111.00	79.00	0.64
MVDE	1	902.12 ± 869.00	1294.88 ± 2.55	96.85 ± 14.62	−99.34 ± 2.28	0.60 ± 0.10
	2	395.43 ± 6.09	1975.5 ± 4.80	76.73 ± 16.77	−80.09 ± 1.48	0.49 ± 0.00
μJADE	1	4078.24 ± 330.07	1308.41 ± 11.55	167.56 ± 24.49	−98.37 ± 2.87	0.73 ± 0.01
	2	2194.95 ± 5608.97	1969.38 ± 3.01	96.41 ± 33.85	−80.54 ± 2.46	0.67 ± 0.24

Table 9. *Parameter ranges used in the MDE variants inversion of KTB anomaly and comparison model parameters estimated by MDE variants and others using inclined sheet as source.*

Algorithms	Sources	K (mVm)	D (m)	h (m)	a (m)	θ (°)
Search spaces	1	10:200	800:1100	10:500	10:2000	40:80
	2	10:200	1300:1800	10:500	10:2000	60:180
VFSA (Biswas 2017)	1	73.50	998.60	371.80	524.60	139.60
	2	79.00	1472.10	298.20	394.80	134.20
WOA (Gobashy *et al.* 2019)	1	58.63	632.70	468.54	739.25	40.02
	2	54.53	1173.56	308.21	655.92	153.76
MVDE	1	74.98 ± 21.05	505.52 ± 2.98	447.09 ± 56.80	429.13 ± 61.95	79.11 ± 1.64
	2	120.06 ± 5.39	1224.99 ± 6.82	134.82 ± 58.10	128.86 ± 8.67	103.95 ± 61.95
μJADE	1	67.08 ± 1.44	500.00 ± 0.01	556.99 ± 18.13	530.23 ± 13.48	80.00 ± 0.00
	2	91.67 ± 4.93	1271.08 ± 10.45	154.15 ± 11.34	149.84 ± 18.20	117.76 ± 1.84

Table 10. *Parameter ranges used in the MDE variants inversion of LUSI embankment SP anomaly, and comparison MDE variants inversion results with parameters revealed by several researchers (Sungkono and Warnana 2018; Abdelazeem et al. 2019).*

Parameter	Sources	K (mVm)	D (m)	h (m)	θ (°)	q
Search space	1	−600:−100	0:75	00:30	0.125	0.3:1.6
	2	−600:−100	75:110	00:30	0.125	0.3:1.6
	3	100:600	150:215	00:30	0.125	0.3:1.6
	4	−600:−100	200:300	00:30	0.125	0.3:1.6
BHA (Sungkono and Warnana 2018)	1	−412.99 ± 4.47	46.46 ± 0.60	16.16 ± 0.35	104.07 ± 1.85	1.06 ± 0.00
	2	−386.59 ± 11.10	99.69 ± 0.39	15.76 ± 0.59	85.88 ± 2.88	1.14 ± 0.01
	3	480.60 ± 27.95	154.93 ± 0.76	25.61 ± 0.36	140.23 ± 2.02	1.01 ± 0.01
	4	−563.42 ± 10.49	268.04 ± 2.10	18.93 ± 0.43	103.75 ± 6.47	1.10 ± 0.00
WOA (Abdelazeem *et al.* 2019)	1	−197.47	32.65	18.68	63.17	0.9
	2	−460.80	102.56	14.22	104.4	1.18
	3	264.56	152.29	30.21	139.06	0.88
	4	−498.57	262.59	28.66	77.53	1.05
MVDE	1	−653.22 ± 61.91	41.35 ± 1.38	18.25 ± 1.34	81.89 ± 3.26	1.13 ± 0.02
	2	−595.84 ± 39.32	92.03 ± 1.86	13.27 ± 1.46	39.04 ± 10.10	1.28 ± 0.06
	3	850.07 ± 54.66	150.59 ± 0.87	22.51 ± 2.24	127.46 ± 3.05	1.11 ± 0.01
	4	−303.87 ± 72.05	267.85 ± 1.86	19.37 ± 1.29	103.00 ± 7.47	0.98 ± 0.04
μJADE	1	−655.59 ± 14.73	48.07 ± 0.08	14.62 ± 0.21	114.04 ± 0.059	1.18 ± 0.00
	2	−675.71 ± 12.81	109.85 ± 0.05	15.31 ± 0.81	134.25 ± 2.73	1.23 ± 0.00
	3	894.65 ± 4.97	152.40 ± 2.68	28.05 ± 1.86	136.00 ± 4.62	1.10 ± 0.01
	4	−674.09 ± 14.03	281.05 ± 0.29	20.25 ± 0.38	141.63 ± 1.18	1.07 ± 0.00

decreases, h will also decreases. Furthermore, the number of evaluations in MDE is evaluated and compared using GPA and GNA. The number of evaluations for MDE variants and GPA are 10,000 and 50 million, correspondingly. It can be seen that MDE variants require lesser evaluation number compared to GPA.

Furthermore, figure 9 is a well fitted curve of the observed KTB anomaly and the calculated model using inclined sheet approach with misfit equal to 1.72% and 2.03% for MVDE and μJADE (better than WOA which has 4.62%), respectively, while table 8 shows the model parameters and its uncertainty revealed by limit acceptability approach with MDE variants. The results is compared with several approaches including VFSA (Biswas 2017) and WOA (Gobashy *et al.* 2019). The MVDE and μJADE model parameter results show that electric dipole moment, the horizontals and the depths of sheet centers are comparable to VFSA, while other parameters fall quite far. In addition, WOA results for source 2 is irrelevant to the geological model because the model parameter is reliable when $h > a \sin\theta$ (Biswas and Sharma 2014b). Meanwhile, about 10,500 numbers of evaluations are needed for both MVDE and μJADE algorithm. On the contrary, WOA and VFSA require 350,000 and 1 billion evaluation numbers making them slower than MDE variants.

5.6 *Vilarelho da Raia anomaly, Portugal*

SP anomaly from the Vilarelho da Raia field data is characterized by a natural spring of CO_2-rich mineral water which is controlled and connected with the Hercynian Fault systems. Monteiro Santos *et al.* (2002) suggest that the SP anomaly contains fractures correlated to the upflow of water in the thermal hot springs area, white aquifer, at a depth between 50 and 150 m. Therefore, several researchers (Monteiro Santos 2010; Di Maio *et al.* 2019) use multiple simple polarized structure model as sources for the SP anomaly inversion, while others (Biswas and Sharma 2014b; Di Maio *et al.* 2019) applied a multiple sheet type structure for forward modelling.

Figures 11 and 12(a) show two profiles that are measured at the Vilarelho da Raia area, Portugal (Monteiro Santos *et al.* 2002). The SP anomaly was analyzed using PSO (Monteiro Santos 2010) and GPA (Di Maio *et al.* 2019) with the assumption that the anomaly contains two polarized structures. Recently, the Vilarelho da Raia SP anomaly has been also inverted using VFSA (Biswas and Sharma 2014b) and GPA (Di Maio *et al.* 2019) via

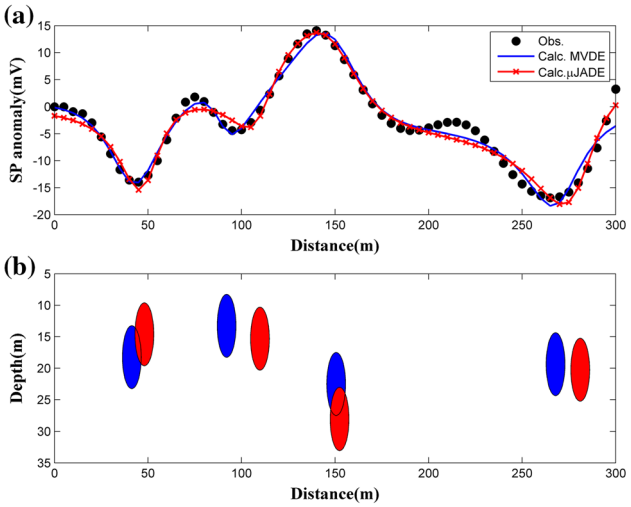

Figure 13. Field SP data from the LUSI anomaly (Sungkono and Warnana 2018), Indonesia, inversed using MDE with the sources determined by using simple polarization structures; (**a**) comparison between field data and model response from inversion results using MVDE and μJADE; (**b**) subsurface structure for multiple bodies revealed by MVDE (blue) and μJADE (red).

four sheet-type structures as causative sources. Furthermore, MDE variants processes use two polarized structures and four sheet-type structures in order to give a decent fit between observed and calculated SP anomalies. In this process, 7 and 8 populations are applied for MVDE and μJADE algorithms which use 10,500 of NFE each.

Figure 14 represents the DE inversion response for Vilarelho da Raia field anomaly, which shows a quite worthy fit with the data as a sign for the parameters of the MDE variants inversion model and considered suitable for recovering the SP data. The MDE results are presented in table 11, which show that the sources in MDE variants are also compared with sources revealed by PSO and GPA. Table 11 establishes that for almost every parameter except for depths and polarization amplitudes, the SP parameters are in a good agreement. The two values resulted by MDE variants are generally higher than GPA results, this is generally caused by the depth of anomaly sources which have higher positive correlation with the polarization amplitude (Biswas and Sharma 2015). Although the shape factors of MDE results have a major difference in value with the others, the entire shape factors for all sources and entire algorithms indicate as semi-infinite vertical cylinder for both structures. Subsequently, MDE results using multiple polarized structures are supported with the interpretation by previous authors (Monteiro Santos 2010; Di Maio *et al.* 2019).

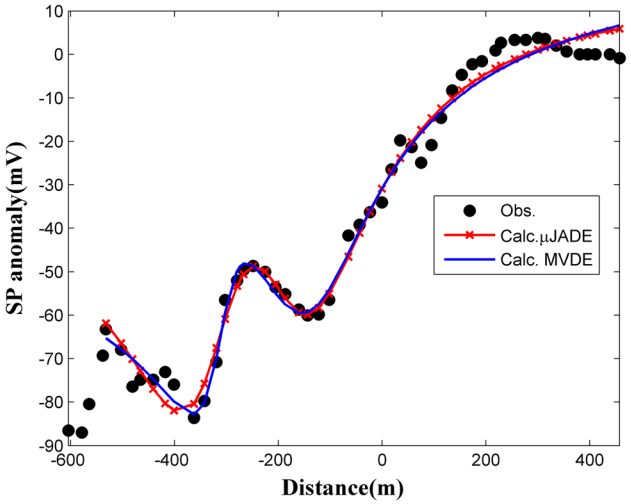

Figure 14. Comparison between observed SP data from the Vilarelho da Raia anomaly (Northern Portugal) (Monteiro Santos *et al.* 2002) and calculated of SP data using MVDE and μJADE with two sources derived by simple polarized structure.

Recently, the Vilarelho da Raia SP anomaly has also been interpreted by some authors (Biswas and Sharma 2014b; Di Maio *et al.* 2019) using GOM. The anomaly is considered to contain four inclined sheet structures in order to give better characterization of the SP anomaly. Thus, MDE variants have been analyzed using the assumption where the SP response from MVDE and μJADE results (table 12 and figure 15b) is close to the observed SP anomaly (the objective function is 0.06 and 0.05 for MVDE and μJADE, respectively) (figure 15a). Table 12 shows inversion results of MDE and other algorithms including VFSA and GPA. The results show that the locations of the central sources for anomalies 2 and 3 are in a good agreement with those revealed by previous researchers (Monteiro Santos *et al.* 2002; Monteiro Santos 2010; Biswas and Sharma

Table 11. *Parameter ranges used in the MDE variants inversion of Vilarelho da Raia anomaly and comparison model parameters estimated by MDE variants and others using simple polarized as source.*

Methods	Sources	K (mVm)	D (m)	h (m)	θ (°)	q
Ranges	1	−500:500	−500:−250	0.5:150	5:180	0.01:1.5
	2	−1200:50	−260:0	0.5:150	5:150	0.01:1.5
PSO (Monteiro Santos 2010)	1	461.70	−383.50	20.00	95.03	0.10
	2	−1200.00	−133.30	3.70	89.49	0.10
GPA (Di Maio *et al.* 2019)	1	−13.49	−340.34	18.06	110.33	0.36
	2	−6.05	−120.50	38.14	91.59	0.15
MVDE	1	−475.04 ± 10.91	−312.11 ± 3.78	53.26 ± 5.95	178.95 ± 2.31	0.81 ± 0.01
	2	−30.8 ± 1.90	−136.07 ± 5.94	134.48 ± 10.83	102.67 ± 2.47	0.41 ± 0.00
μJADE	1	−499.89 ± 1.11	−335.66 ± 63.90	110.92 ± 15.09	141.36 ± 35.15	0.70 ± 0.01
	2	−1199.98 ± 0.61	−157.90 ± 61.63	143.27 ± 2.36	72.48 ± 29.99	0.77 ± 0.05

Table 12. *Parameter ranges used in the MDE variants inversion of Vilarelho da Raia anomaly and comparison model parameters estimated by MDE variants and others using inclined sheet as source.*

Algorithms	Sources	K (mVm)	D (m)	h (m)	a (m)	θ (°)
Search spaces	1	0:40	−500:−400	10:150	20:100	5:180
	2	0:40	−400:−300	10:150	20:100	5:180
	3	0:40	−200:−34	10:150	20:100	5:180
	4	0:50	−24:300	10:150	20:100	5:180
VFSA (Biswas and Sharma 2014b)	1	31.4	−467.23	122.29	51.38	76.78
	2	13.4	−389.71	60.66	40.34	122.92
	3	13.2	−115.66	111.39	37.42	77.92
	4	2.9	150.56	31.57	73.6	5.29
GPA (Di Maio *et al.* 2019)	1	26.38	−488.00	122.71	62.8	86.06
	2	13.68	−349.02	98.34	69.16	85.36
	3	17.87	−112.43	119.53	69.64	77.82
	4	18.25	116.57	69.51	16.48	24.84
MVDE	1	48.06 ± 3.31	−491.06 ± 13.14	142.63 ± 9.93	81.62 ± 7.95	38.11 ± 2.30
	2	18.46 ± 2.37	−350.35 ± 25.45	124.84 ± 27.66	91.55 ± 9.63	62.39 ± 12.72
	3	17.06 ± 8.24	−186.33 ± 13.32	65.52 ± 12.47	45.79 ± 22.59	29.54 ± 12.19
	4	11.97 ± 3.10	47.34 ± 27.42	141.69 ± 10.62	157.40 ± 6.61	88.82 ± 18.64
μJADE	1	32.84 ± 10.73	−455.09 ± 45.47	149.44 ± 3.98	64.42 ± 19.45	106.55 ± 25.51
	2	17.50 ± 5.60	−350.77 ± 38.03	123.08 ± 28.82	63.30 ± 22.48	89.03 ± 12.13
	3	17.84 ± 3.87	−113.34 ± 31.02	95.22 ± 23.53	50.14 ± 13.81	105.76 ± 10.08
	4	15.41 ± 3.21	87.27 ± 21.35	134.27 ± 28.32	45.95 ± 14.56	139.12 ± 8.74

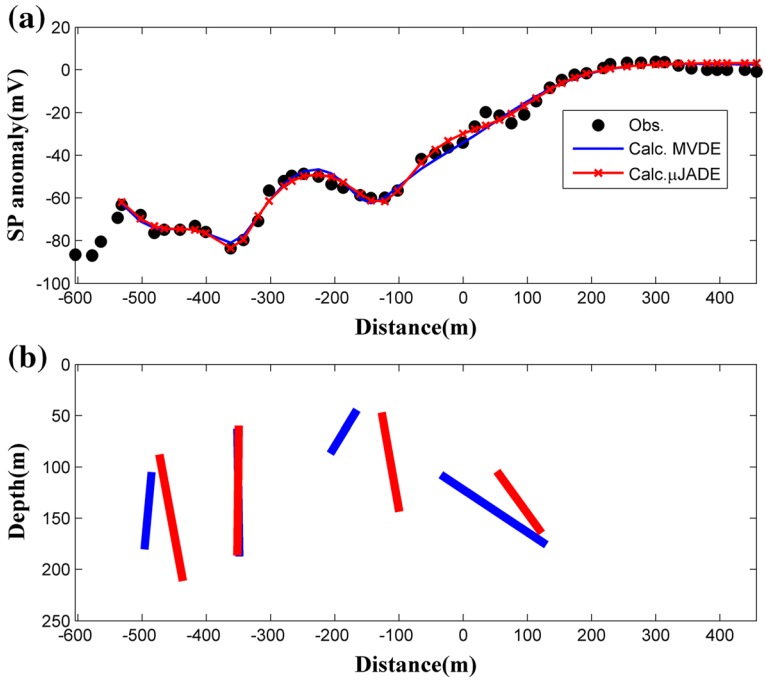

Figure 15. Field SP data from the Vilarelho da Raia anomaly (Monteiro Santos *et al.* 2002) inversed using MDE variants with fourth sources determined using inclined sheet structures; (**a**) comparison between field data and model response resulted by MVDE and μJADE, (**b**) subsurface structure for multiple bodies revealed by MVDE (blue) and μJADE (red).

2014b; Di Maio *et al.* 2019) and also comparable with table 11. Furthermore, through comparison between figures 14 and 15(a), it can be seen that multiple inclined sheet structure is suitable for the Vilarelho da Raia SP curves interpretation.

In order to appraise the efficiency of MDE compared with VFSA and GPA, forward modelling is required for each algorithm to be evaluated. Based on several researchers (Biswas and Sharma 2014b; Di Maio *et al.* 2019), the number of forward computations for the inversion of Vilarelho da Raia anomaly is known, where VFSA and GPA need 1 and 50 million forward computations, individually, while MVDE and μJADE require 10,500 and 1,200, respectively. Thus, it can be seen that MDE is much more efficient than GPA and VFSA.

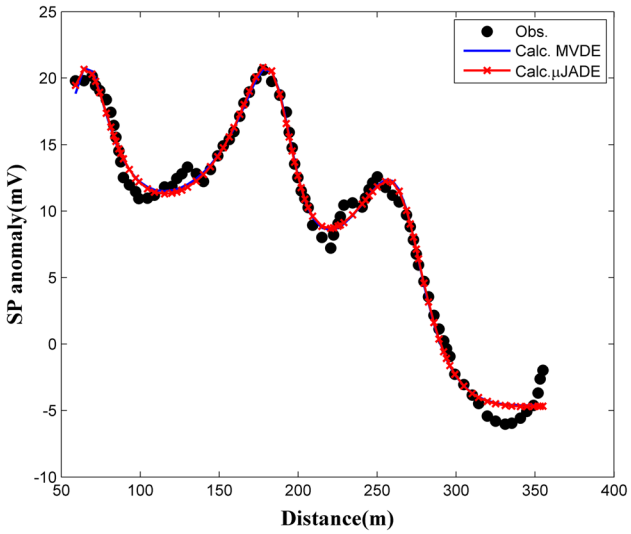

Figure 16. Comparison between observed SP data from the Karakoç creek anomaly (Göktürkler *et al.* 2008) and calculated data through inversed process using MDE and μJADE using consideration three simple polarized anomalies.

5.7 *Karakoç creek, Turkey*

The SP data was acquired from southwest of the Çubukludağ graben, southwest of İzmir, western Turkey. The observed SP data is for an alluvial aquifer study in September 2006 by Göktürkler *et al.* (2008). The observed SP data in line 4 (figure 16) is analyzed using simple polarized approach with the assumption that the observed data contain four anomalies; however, the last anomaly remains incomplete. Consequently, analyzed data in this line takes in consideration of three anomalies. The SP anomalies are caused by near surface fluid flow phenomena. Consequently, table 13 is used as a search space in the inversion process.

In order to find PDM in the SP model, μJADE and MVDE algorithms are processed through 20,000 numbers of evaluation for each algorithms

Table 13. *Parameter ranges used in the MDE variants inversion of Karakoç creek anomaly and model parameters estimated by MDE variants using simple polarized as source.*

Algorithms	Sources	K (mVm)	D (m)	h (m)	θ (°)	q
Search spaces	1	−50:300	60:150	0.1:28	5:180	0.5:1.8
	2	−50:300	140:230	0.1:28	5:180	0.5:1.8
	3	−50:300	230:360	0.1:28	5:180	0.5:1.8
MVDE	1	270.10 ± 15.99	63.05 ± 0.91	18.44 ± 1.63	74.37 ± 4.71	0.99 ± 0.01
	2	210.42 ± 27.92	187.81 ± 1.00	21.49 ± 2.07	131.25 ± 2.92	0.93 ± 0.01
	3	129.39 ± 27.62	268.91 ± 0.87	24.78 ± 1.42	133.37 ± 1.18	0.83 ± 0.03
μJADE	1	298.64 ± 9.07	65.86 ± 7.16	22.11 ± 1.44	88.97 ± 16.40	0.99 ± 0.01
	2	293.97 ± 39.75	186.73 ± 2.29	22.69 ± 3.09	127.20 ± 7.10	0.97 ± 0.03
	3	99.56 ± 28.07	271.31 ± 3.22	25.00 ± 0.05	136.28 ± 6.85	0.79 ± 0.05

with 8 and 5 population size, respectively. The algorithm is executed to 10 independent runs to be then selected to find the lowest objective function. The best fit of both algorithms is presented in figure 16. The figures show a good fit between observed and calculated SP data from μJADE and MVDE, except in the last anomaly because the data is considered incomplete.

Furthermore, the limit acceptability method, or the objective function threshold can be applied to generate PDM. It means that the model parameters of the objective function lower than the threshold value become PDM. In the inversion, 0.15 is set as the threshold value. The median and their uncertainty of the PDM acquired from the threshold are presented in table 13. The table indicates that the anomalies located by both μJADE and MVDE algorithm are similar about 62–72, 186–189 and 268–275 m in distance and 17.5–25 m in depth. The inversion result is supported by inversion of 2D resistivity results which indicate that the aquifer in the alluvial is located above 20 m (Göktürkler *et al.* 2008). Furthermore, the second and third anomalies of SP data are correlated with low resistivity zones.

6. Conclusion

A recently proposed micro-differential evolution (MDE) variant has been implemented to provide quantitative interpretation of mono and multiple SP anomalies with simple geometry namely simple polarized and inclined sheet. MDE is a differential evolution with micro-population, which is robust and fast to reach convergence while requiring little populations, and produces reliable results in the inversion of single and multiple anomalies of SP data. Both MDE variants, namely MVDE and μJADE have been tested over synthetics and fields of SP anomalies for showing the performance of the algorithm. The fields of SP anomaly from landslide and ground water investigations, embankment stability identification, mineral exploration, and tracing shear zones demonstrated that MDE results are generally faster compared to the results revealed by the most common global optimization algorithms, namely GA, PSO, standard DE, GPA, WOA, BHA, and VFSA. MDE variants for SP data inversion commonly generate the model parameters which appropriate the availability of geological information of the survey area. Finally, it can be concluded that the MDE variants are able to determine 10–20 model parameters of synthetic and field SP data using 5–8 populations, a task impossible to be solved by standard DE. The discovery of MDE will provide new chances for imaging high-dimensional model (2D or 3D subsurface) from geophysical data.

Acknowledgement

The research was supported by Institute for Research and Community Services of Institut Teknologi Sepuluh Nopember, Surabaya.

References

Abdelazeem M, Gobashy M, Khalil M H and Abdrabou M 2019 A complete model parameter optimization from self-potential data using Whale algorithm; *J. Appl. Geophys.* **170** 103825.

Agarwal B N P and Srivastava S 2009 Analyses of self-potential anomalies by conventional and extended Euler deconvolution techniques; *Comput. Geosci.* **35** 2231–2238.

Arora T, Linde N, Revil A and Castermant J 2007 Non-intrusive characterization of the redox potential of landfill leachate plumes from self-potential data; *J. Contam. Hydrol.* **92** 274–292.

Balkaya Ç 2013 An implementation of differential evolution algorithm for inversion of geoelectrical data; *J. Appl. Geophys.* **98** 160–175.

Balkaya Ç, Ekinci Y L, Göktürkler G and Turan S 2017 3D non-linear inversion of magnetic anomalies caused by prismatic bodies using differential evolution algorithm; *J. Appl. Geophys.* **136** 372–386.

Biswas A 2017 A review on modeling, inversion and interpretation of self-potential in mineral exploration and tracing paleo-shear zones; *Ore Geol. Rev.* **91** 21–56.

Biswas A and Sharma S P 2015 Interpretation of self-potential anomaly over idealized bodies and analysis of ambiguity using very fast simulated annealing global optimization technique; *Surf. Geophys.* **13** 179–195.

Biswas A and Sharma S P 2014a Integrated geophysical studies to elicit the subsurface structures associated with Uranium mineralization around South Purulia Shear Zone, India: A review; *Ore Geol. Rev.* **72(2)** 1307–1326.

Biswas A and Sharma S P 2014b Optimization of self-potential interpretation of 2-D inclined sheet-type structures based on very fast simulated annealing and analysis of ambiguity; *J. Appl. Geophys.* **105** 235–247.

Biswas A and Sharma S P 2014c Resolution of multiple sheet-type structures in self-potential measurement; *J. Earth Syst. Sci.* **123** 809–825.

Brown C, Jin Y, Leach M and Hodgson M 2016 µJADE: Adaptive differential evolution with a small population; *Soft Comput.* **20** 4111–4120.

Byrdina S, Rücker C, Zimmer M, Friedel S and Serfling U 2012 Self potential signals preceding variations of fumarole activity at Merapi volcano, Central Java; *J. Volcanol. Geotherm. Res.* **215–216** 40–47.

Candra A D, Srigutomo W, Sungkono and Santosa B J 2014 A complete quantitative analysis of self-potential anomaly using singular value decomposition algorithm; In: *IEEE International Conference on Smart Instrumentation, Measurement and Applications (ICSIMA)*, pp. 1–4.

Di Maio R, Piegari E, Rani P, Carbonari R, Vitagliano E and Milano L 2019 Quantitative interpretation of multiple self-potential anomaly sources by a global optimization approach; *J. Appl. Geophys.* **162** 152–163.

Di Maio R, Rani P, Piegari E and Milano L 2016 Self-potential data inversion through a genetic-price algorithm; *Comput. Geosci.* **94** 86–95.

Ekinci Y L, Balkaya Ç and Göktürkler G 2020 Global optimization of near-surface potential field anomalies through metaheuristics; In: *Advances in Modeling and Interpretation in Near Surface Geophysics* (eds) Biswas A and Sharma S P Springer Geophysics, Springer, Cham, pp. 155–188.

Ekinci Y L, Balkaya Ç and Göktürkler G 2019 Parameter estimations from gravity and magnetic anomalies due to deep-seated faults: Differential evolution versus particle swarm optimization; *Turk. J. Earth Sci.* **28** 860–881.

Ekinci Y L, Balkaya Ç, Göktürkler G and Turan S 2016 Model parameter estimations from residual gravity anomalies due to simple-shaped sources using differential evolution algorithm; *J. Appl. Geophys.* **129** 133–147.

Ekinci Y L, Özyalın Ş, Sındırgı P, Balkaya Ç and Göktürkler G 2017 Amplitude inversion of the 2D analytic signal of magnetic anomalies through the differential evolution algorithm; *J. Geophys. Eng.* **14** 1492–1508.

El-Kaliouby H M and Al-Garni M A 2009 Inversion of self-potential anomalies caused by 2D inclined sheets using neural networks; *J. Geophys. Eng.* **6** 29.

Fajriani Srigutomo W and Pratomo P M 2017 Interpretation of self-potential anomalies for investigating fault using the Levenberg–Marquardt method: A study case in Pinggirsari, West Java, Indonesia; *IOP Conf. Ser. Earth Environ. Sci.* **62** 012004.

Fernández-Martínez J L, Pallero J L G, Fernández-Muñiz Z and Pedruelo-González L M 2014a The effect of noise and Tikhonov's regularization in inverse problems. Part II: The nonlinear case; *J. Appl. Geophys.* **108** 186–193.

Fernández-Martínez J L, Pallero J L G, Fernández-Muñiz Z and Pedruelo-González L M 2014b The effect of noise and Tikhonov's regularization in inverse problems. Part I: The linear case; *J. Appl. Geophys.* **108** 176–185.

Gobashy M, Abdelazeem M, Abdrabou M and Khalil M H 2019 Estimating model parameters from self-potential anomaly of 2D inclined sheet using whale optimization algorithm: Applications to mineral exploration and tracing shear zones; *Nat. Resour. Res.* **29** 499–519.

Göktürkler G and Balkaya Ç 2012 Inversion of self-potential anomalies caused by simple-geometry bodies using global optimization algorithms; *J. Geophys. Eng.* **9** 498–507.

Göktürkler G, Balkaya Ç, Erhan Z and Yurdakul A 2008 Investigation of a shallow alluvial aquifer using geoelectrical methods: A case from Turkey; *Environ. Geol.* **54** 1283–1290.

Husein A, Sungkono, Wijaya A and Hadi S 2014 Subsurface monitoring of P.79–P.82 LUSI Embankment using GPR method to locate subsidence and possible failure; In: *15th International Conference on Ground Penetrating Radar (GPR),* Brussels, Belgium, pp. 268–273.

Jardani A, Revil A and Dupont J P 2006 Self-potential tomography applied to the determination of cavities; *Geophys. Res. Lett.* **33** L13401.

Lapenna V, Lorenzo P, Perrone A, Piscitelli S, Sdao F and Rizzo E 2003 High-resolution geoelectrical tomographies in the study of Giarrossa landslide (southern Italy); *Bull. Eng. Geol. Environ.* **62** 259–268.

Li X and Yin M 2012 Application of differential evolution algorithm on self-potential data; *PLoS ONE* **7** e51199.

Mehanee S A 2015 Tracing of paleo-shear zones by self-potential data inversion: Case studies from the KTB, Rittsteig, and Grossensees graphite-bearing fault planes; *Earth Planets Space* **67** 14.

Mehanee S A 2014 An efficient regularized inversion approach for self-potential data interpretation of ore exploration using a mix of logarithmic and non-logarithmic model parameters; *Ore Geol. Rev.* **57** 87–115.

Monteiro Santos F A 2010 Inversion of self-potential of idealized bodies' anomalies using particle swarm optimization; *Comput. Geosci.* **36** 1185–1190.

Monteiro Santos F A, Almeida E P, Castro R, Nolasco R and Mendes-Victor L 2002 A hydrogeological investigation using EM34 and SP surveys; *Earth Planets Space* **54** 655–662.

Moore J R, Boleve A, Sanders J W and Glaser S D 2011 Self-potential investigation of moraine dam seepage; *J. Appl. Geophys.* **74** 277–286.

Olguín-Carbajal M, Alba E and Arellano-Verdejo J 2013 Micro-differential evolution with local search for high

dimensional problems; In: *2013 IEEE Congress on Evolutionary Computation*, pp. 48–54.

Pallero J L G, Fernández-Martínez J L, Bonvalot S and Fudym O 2015 Gravity inversion and uncertainty assessment of basement relief via particle swarm optimization; *J. Appl. Geophys.* **116** 180–191.

Pekşen E, Yas T, Kayman A Y and Özkan C 2011 Application of particle swarm optimization on self-potential data; *J. Appl. Geophys.* **75** 305–318.

Ramadhani I and Sungkono 2019 A new approach to model parameter determination of self-potential data using memory-based hybrid dragonfly algorithm; *Int. J. Adv. Sci. Eng. Inf. Technol.* **9** 1772–1782.

Ramadhany B, Sungkono, Rohman A, Warnana D D and Lestari S 2018 Comprehensive analysis of microtremor data to identify potential landslide (Study case: KM23 Ponorogo–Trenggalek Road); In: *The EAGE-HAGI 1st Asia Pacific Meeting on Near Surface Geoscience and Engineering.*

Reddi A G B, Madhusudan I C, Sarkar B and Sharma J K 1982 An album of geophysical responses from base metal belts of Rajasthan and Gujarat (Calcutta: Geological Survey of India); Miscellaneous Publication.

Ren X, Chen Z and Ma Z 2010 Differential evolution using smaller population; In: *2010 Second International Conference on Machine Learning and Computing,* pp. 76–80.

Ronkkonen J, Kukkonen S and Price K V 2005 Real-parameter optimization with differential evolution; In: *The 2005 IEEE Congress on Evolutionary Computation*, **1** 506–513.

Salehinejad H, Rahnamayan S and Tizhoosh H R 2017 Micro-differential evolution: Diversity enhancement and a comparative study; *Appl. Soft. Comput.* **52** 812–833.

Salehinejad H, Rahnamayan S and Tizhoosh H R 2016 Exploration enhancement in ensemble micro-differential evolution; In: *2016 IEEE Congress on Evolutionary Computation (CEC)*, pp. 63–70.

Saracco G, Labazuy P and Moreau F 2004 Localization of self-potential sources in volcano-electric effect with complex continuous wavelet transform and electrical tomography methods for an active volcano; *Geophys. Res. Lett.* **31** L12610.

Srigutomo W, Agustine E and Zen M H 2006 Quantitative analysis of self-potential anomaly: Derivative analysis, least-squares method and non-linear inversion; *Indones. J. Phys.* **17** 49–55.

Stoll J, Bigalke J and Grabner E W 1995 Electrochemical modelling of self-potential anomalies; *Surv. Geophys.* **16** 107–120.

Sundararajan N and Srinivas Y 1996 A modified Hilbert transform and its application to self-potential interpretation; *J. Appl. Geophys.* **36** 137–143.

Sungkono 2020 Robust interpretation of single and multiple self-potential anomalies via flower pollination algorithm; *Arab. J. Geosci.* **13** Article ID 100, 1–16.

Sungkono, Feriad, Y, Husein A, Prasetyo H, Charis M, Irawan D, Rochman J P G N, Bahri A S and Santosa B J 2018 Assessment of Sidoarjo mud flow embankment stability using very low frequency electromagnetic method; *Environ. Earth Sci.* **77** 196.

Sungkono, Husein A, Prasetyo H, Bahri A S, Monteiro Santos F A and Santosa B J 2014 The VLF-EM imaging of potential collapse on the LUSI embankment; *J. Appl. Geophys.* **109** 218–232.

Sungkono and Santosa B J 2015 Differential evolution adaptive metropolis sampling method to provide model uncertainty and model selection criteria to determine optimal model for Rayleigh wave dispersion; *Arab. J. Geosci.* **8** 7003–7023.

Sungkono and Warnana D D 2018 Black hole algorithm for determining model parameter in self-potential data; *J. Appl. Geophys.* **148** 189–200.

Tlas M and Asfahani J 2013 An approach for interpretation of self-potential anomalies due to simple geometrical structures using fair function minimization; *Pure Appl. Geophys.* **170** 895–905.

Vrugt J A and Beven K 2018 Embracing equifinality with efficiency: Limits of acceptability sampling using the DREAM (LOA) algorithm; *J. Hydrol.* **559** 954–971.

Yang X S 2014 *Nature-Inspired Metaheuristic Algorithms*; Luniver Press.

Zhang J and Sanderson A C 2009 JADE: adaptive differential evolution with optional external archive; *IEEE Trans. Evol. Comput.* **13** 945–958.

Corresponding editor: Arkoprovo Biswas